

## Original Article

## Synthesis of significant nitroimidazole-triazole-pyridine hybrids and their molecular modeling as antimicrobial agents

Maha Ali Aljowni<sup>a</sup>, Hind A. Siddiq<sup>b</sup>, Rabah N Alsulami<sup>c</sup>, Gadeer R. S. Ashour<sup>d</sup>, Nawaa Ali H. Alshammari<sup>e</sup>, Adel I. Alalawy<sup>f</sup>, Wael M. M. Alamoudi<sup>c</sup>, Hana M. Abumelha<sup>g,\*</sup>

<sup>a</sup>Department of Chemistry, Faculty of Science, University of Tabuk, Saudi Arabia

<sup>b</sup>Department of Physical Sciences, Chemistry Division, College of Science, Jazan University, Jazan, Saudi Arabia.

<sup>c</sup>Department of Biology, Faculty of Science, Umm Al Qura University, Makkah, Saudi Arabia

<sup>d</sup>Department of Chemistry, College of Science, Umm Al-Qura University, Makkah, Saudi Arabia

<sup>e</sup>Department of Chemistry, College of Science, Northern Border University, Arar, Saudi Arabia

<sup>f</sup>Department of Biochemistry, Faculty of Science, University of Tabuk, Saudi Arabia

<sup>g</sup>Department of Chemistry, College of Science, Princess Nourah bint Abdulrahman University, Riyadh, Saudi Arabia

## ARTICLE INFO

**Keywords:**  
Azidoacetyl-imidazole  
DFT modelling  
Docking  
Imidazole-triazole-pyridine  
SwissADME

## ABSTRACT

A series of nitroimidazole-triazole hybrids **7a-d** and **10a-d** have been synthesized through the Huisgen cycloaddition of 1-(2-azidoacetyl)-2-methyl-5-nitro-1*H*-imidazole (**3**) with 2-((4-propargyloxy)benzylidene) malononitrile (**4**) or ethyl 2-cyano-3-((4-propargyloxy)phenyl) acrylate (**8**), followed by cyclization of imidazole-triazole compounds (**5** and **9**) with *N*-aryl cyanoacetamides **6a-d**. The DFT calculations for the synthesized nitroimidazole-based hybrids revealed comparable twisted configurations and similar Highest occupied molecular orbitals (HOMO)-lowest unoccupied molecular orbital (LUMO) constructions. Consequently, their energy gap ranged from 2.93 to 3.33 eV, where analogues **7b** and **5** exhibited the utmost and least values, respectively. In addition, the antimicrobial effectiveness of the prepared nitroimidazole-based hybrids against Gram(+ve), Gram(-ve), and fungal strains were assessed using MIC and IZ assays. Imidazole-triazole hybrids **7a**, **7b**, and **10d** displayed the highest activity, particularly against *S. aureus*, *B. subtilis*, and *E. coli* (minimum inhibitory concentrations (MIC) = 3.125-6.25 µg.mL<sup>-1</sup>), comparable to the reference antibiotics. However, nitroimidazole-triazole hybrid **9** demonstrated a robust fungicidal effect on *C. albicans* (MIC = 3.125 µg.mL<sup>-1</sup>), comparable to cycloheximide. The molecular docking study was performed to evaluate interactions of the manufactured series with the target protein (PDB: 1BDD). The hybrids **5** and **10d** presented the maximum binding affinities (*S* = -7.1215 and -7.2123 kcal.mol<sup>-1</sup>). These findings suggest that nitroimidazole-hybrids, particularly **10d** and **5**, represented promising scaffolds for further development due to their strong binding affinities and diverse interaction profiles. Furthermore, the Swiss Absorption, distribution, metabolism, and excretion (ADME) study provided an in-depth pharmacokinetic evaluation of the new nitroimidazole hybrids, a robust tool for predicting drug-likeness and bioavailability. Hybrids **5** and **9** exhibited favorable solubility with low molecular weights, while hybrids **7a-d** and **10a-d** showed moderate solubility but higher molecular weights and increased Lipinski violations. The bioavailability scores showed moderate to low, with nitroimidazole-hybrids **5** and **9**. These pharmacokinetic results offered valuable insights into the drug-likeness and potential therapeutic pertinency of these hybrids.

## 1. Introduction

Undoubtedly, antimicrobial resistance became one of the most demanding targets in recent drugs, threatening the effectiveness of the drugs it depends on and driving scientists to search for new methods to struggle infections [1]. New heterocyclic compounds have attracted the attention of researchers owing to their potential to function as disinfectants. Among these, nitroimidazole hybrids have been recombined into a specific class of antimicrobial drugs (Figure 1) [2]. Their lone structure, which includes a nitro group added to associate with the indazole moiety, gives them bacterial-killer power to fight

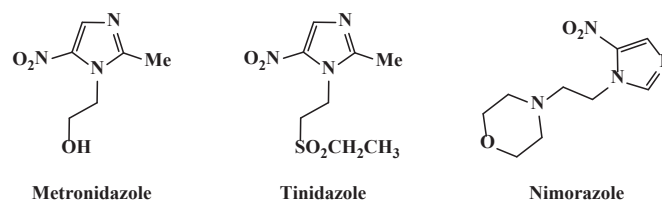


Figure 1. Chemical structures of nitroimidazole antibiotics.

## \*Corresponding author:

E-mail address: hmabumelha@pnu.edu.sa (H. Abumelha)

Received: 21 February, 2025 Accepted: 15 December, 2025 Epub Ahead of Print: 06 March, 2026 Published: 02 May, 2026

DOI: 10.25259/AJC\_179\_2025

This is an open-access article distributed under the terms of the Creative Commons Attribution-Non Commercial-Share Alike 4.0 License, which allows others to remix, transform, and build upon the work non-commercially, as long as the author is credited and the new creations are licensed under the identical terms.

microbes [3]. Meanwhile, much research on the nitroimidazole hybrids was conducted, broadly against their antibacterial, antitubercular, antifungal, and antiprotozoal properties [4]. Their effectiveness may be attributed to their ability to inhibit the antimicrobial DNA replication and induce oxidative stress by disrupting the formation of deoxyribonucleic acid of the microbes [5]. Nevertheless, the existence of nitroimidazole-hybrids based on the nitro-group showed potent effectiveness as it exhibits a bio-reduction role within the bacterial metabolism, leading to the formation of reactive species that cause an oxidative damage, troublemaking essential cellular formation, and ultimately leading to cell death [6]. Moreover, several heterocyclic rings like triazole and pyridine have exhibited a noteworthy role in the improvement of the antimicrobial efficiency [7]. For example, triazoles are famously recognized for their robust fungal and bacterial inhibitions [8]. In addition, it possesses a five-membered heterocycle containing three nitrogen atoms, which gives it the ability to bind with microbial enzymes and inhibit them through their synthetic pathways. Furthermore, many of the antifungal medicines like fluconazole and itraconazole contain a triazole-ring in their skeletons that plays an effective role through their antimicrobial effectiveness [9]. So, after a triazole-ring is combined with the nitroimidazole-hybrids, it may lead to an improvement in their solubility, bioavailability, and binding interactions with reactive species in the microbial targets, enhancing their overall antimicrobial efficiency [10]. In addition, the strategic utilization of the N-aryl pyridine fragment, accessible via the cyclocondensation of aryl cyanoacetamides, was directed towards making the final hybrids more molecularly diverse and predisposed to bind with the target microbial enzymes. The pyridine ring is a privileged structure in medicinal chemistry that has been shown to play crucial roles in hydrogen bonding and dipole-dipole interactions with microbial enzyme targets [11]. The N-aryl substitution pattern was selected to methodically investigate the influence of different electronic (electron-donating methoxy and electron-withdrawing nitro and chloro groups) and steric properties on antimicrobial activity and pharmacokinetics, a strategy widely applied in structure-activity relationship studies. The existence of the pyridine moiety in antimicrobial agents led to the facility of the drug to penetrate microbial cells, increasing their influence [12]. When the combination between nitroimidazole-hybrids with the pyridine ring can additionally improve the antimicrobial efficiency by increasing electron density around the targeted sites, leading to stronger bindings with bacterial and fungal cells. This collaboration among pyridine and nitroimidazole-hybrids has been discovered in drug developments, yielding auspicious results in the fight against resistant infections [13].

Another key area of this study is to synthesis and explore the synergy between nitroimidazole-hybrids and other heterocyclic nucleuses such as triazole and pyridine. As the demand for standing on their optimized structures through their molecular modeling and docking with the targeted protein. Ongoing studies aim to discover their antimicrobial properties with continued advancements in pharmacokinetic properties, helping to combat some of the most challenging infectious diseases.

## 2. Materials and Methods

Melting points (uncorrected) were acquired using a digital on Esico melting point apparatus. The infrared spectra were taken using a Bruker Invenio-S FTIR spectrometer. The  $^1\text{H}$ - and  $^{13}\text{C}$ -NMR spectra were recorded with a JEOL spectrometer (500 MHz) in  $\text{DMSO}-d_6$  solvent. The mass analyses were measured using a ThermoScientific GC-MS DSQII (at 70 eV). The elemental analyses of C, H, and N were obtained by a Perkin-Elmer 2400 analyzer. Experimental procedures were adapted and improved from earlier published literature procedures [14] with proper citation now elaborated.

### 2.1. 1-(2-Chloroacetyl)-2-methyl-5-nitro-1H-imidazole (2)

A 250 mL conical flask was charged with a suspension of 2-methyl-5-nitro-1H-imidazole (1) (1.90 g, 15 mmol) and potassium carbonate (2.07 g, 15 mmol) in dry acetone (40 mL). To this suspension, chloroacetyl chloride was added dropwise at 5-10°C with stirring for 4 h. The obtained solid after dilution with 50 mL of cold water was

filtered, washed with cold ethanol, and used directly in the next step after drying.

Yield = 2.17 g (71.3%), m.p. = 189-190°C. IR ( $\nu/\text{cm}^{-1}$ ): 1636 (C=N), 1694 (C=O).  $^1\text{H}$  NMR ( $\delta/\text{ppm}$ ): 2.58 (s, 3H, imidazole- $\text{CH}_3$ ), 4.40 (s, 2H,  $\text{CO}-\text{CH}_2-\text{Cl}$ ), 8.04 (s, 1H, imidazole-H). Calculated analysis for  $\text{C}_6\text{H}_6\text{ClN}_3\text{O}_3$  (203.01): C, 35.40; H, 2.97; N, 20.64%. Found: C, 35.52; H, 2.92; N, 20.58%.

### 2.2. 1-(2-Azidoacetyl)-2-methyl-5-nitro-1H-imidazole (3)

A mixture of 1-(2-chloroacetyl)-2-methyl-5-nitro-1H-imidazole (2) (1.62 g, 8 mmol) and sodium azide (0.65 g, 10 mmol) was stirred in dry DMSO (25 mL) at 50°C for 12 h. The mixture was diluted with 50 mL of cold water, and then the organic layer was extracted with ethyl acetate, dried with anhydrous sodium sulphate, and evaporated. The freshly obtained azide compound 3 was directly used in the next step.

Yield = 0.92 g (54.7%), m.p. = 223-224°C. IR ( $\nu/\text{cm}^{-1}$ ): 1698 (C=O), 2108 (-N=N=N).  $^1\text{H}$  NMR ( $\delta/\text{ppm}$ ): 2.58 (s, 3H, imidazole- $\text{CH}_3$ ), 4.38 (s, 2H,  $\text{CO}-\text{CH}_2-\text{N}_3$ ), 8.08 (s, 1H, imidazole-H). Calculated analysis for  $\text{C}_6\text{H}_6\text{N}_6\text{O}_3$  (210.05): C, 34.29; H, 2.88; N, 39.99%. Found: C, 34.18; H, 2.94; N, 39.85%.

### 2.3. 2-(4-((1-(2-(2-Methyl-5-nitro-1H-imidazol-1-yl)-2-oxoethyl)-1H-1,2,3-triazol-4-yl) methoxy)benzylidene)malononitrile (5)

A mixture of 1-(2-azidoacetyl)-2-methyl-5-nitro-1H-imidazole (3) (0.94 g, 4.5 mmol) and 2-((4-propargyloxy)benzylidene)malononitrile (4) [14] (0.83 g, 4 mmol) was dissolved in 30 mL of dimethylformamide (DMF). To the obtained solution, sodium ascorbate (40 mol %) and copper sulphate pentahydrate (20 mol %) had been introduced in sequence. The mixture was stirred at 35-40°C for 12 h and then diluted with 100 mL ice-cold water. The precipitate that formed was collected and washed with 5 mL of ethyl acetate to furnish the precursor, 2-(4-(triazolyl-methoxy)benzylidene)-malononitrile compound 5.

Yield = 1.41 g (84.3%), m.p. = 160-161°C. IR ( $\nu/\text{cm}^{-1}$ ): 1688 (C=O), 2217 (C=N).  $^1\text{H}$  NMR ( $\delta/\text{ppm}$ ): 2.57 (s, 3H, imidazole- $\text{CH}_3$ ), 4.94 (s, 2H,  $\text{N}-\text{CH}_2-\text{CO}$ ), 5.17 (s, 2H,  $\text{O}-\text{CH}_2-\text{triazole}$ ), 6.93 (d,  $J = 8.5$  Hz, 2H), 7.51 (d,  $J = 8.5$  Hz, 2H), 7.90 (s, 1H,  $\text{CH}=\text{C}-\text{CN}$ ), 8.11 (s, 1H, imidazole-H), 8.27 (s, 1H, triazole-H). MS for  $\text{C}_{19}\text{H}_{14}\text{N}_8\text{O}_4$  [ $\text{M}]^+$ :  $m/z = 418.2$  (16.73%). Calculated analysis for  $\text{C}_{19}\text{H}_{14}\text{N}_8\text{O}_4$  (418.11): C, 54.55; H, 3.37; N, 26.78%. Found: C, 54.68; H, 3.43; N, 26.70%.

### 2.4. 1-Aryl 6-amino-3,5-dicyano-4-(4-((1-(2-(2-methyl-5-nitro-1H-imidazol-1-yl)-2-oxoethyl)-1H-1,2,3-triazol-4-yl)methoxy)phenyl)-2-oxo-1,2-dihydropyridine hybrids 7a-d

An RB-flask (100 mL) was charged with a solution of 2-(4-(triazolyl-methoxy)benzylidene)-malononitrile compound 5 (0.83 g, 2 mmol) in 30 mL ethanol and piperidine (0.1 mL). The corresponding N-aryl cyanoacetamide compound 6a, 6b, 6c, or 6d [15] (2 mmol) was added, and the mixture was refluxed for 2 h. The obtained solid was filtered and crystallized from an EtOH/DMF mixture (4:1) to afford the corresponding imidazole-triazole-pyridine hybrids 7a, 7b, 7c, and 7d, respectively.

#### 2.4.1. Imidazole-triazole-pyridine hybrid (7a)

Yield = 0.64 g (55.6%), m.p. = 252-253°C. IR ( $\nu/\text{cm}^{-1}$ ): 1651 (C=O), 1683 (C=O), 2211 (C=N), 3341, 3213 (-NH<sub>2</sub>).  $^1\text{H}$  NMR ( $\delta/\text{ppm}$ ): 2.61 (s, 3H, imidazole- $\text{CH}_3$ ), 4.97 (s, 2H,  $\text{N}-\text{CH}_2-\text{CO}$ ), 5.18 (s, 2H,  $\text{O}-\text{CH}_2-$ ), 7.10 (d,  $J = 8.5$  Hz, 2H), 7.30-7.39 (m, 5H), 7.56 (d,  $J = 8.5$  Hz, 2H), 7.83 (s, 2H,  $\text{NH}_2$ ), 8.08 (s, 1H, imidazole-H), 8.31 (s, 1H, triazole-H).  $^{13}\text{C}$  NMR ( $\delta/\text{ppm}$ ): 13.05 ( $\text{CH}_3$ ), 52.31 ( $-\text{CH}_2-\text{CO}-$ ), 61.28 ( $-\text{O}-\text{CH}_2-$ ), 75.36 (pyridine-C5), 111.48 (pyridine-C3), 114.63 (2 Ar-C), 115.81 (2 C=N), 122.91 (triazole-C5), 126.56 (Ar-C), 128.21 (3 Ar-C), 128.94 (2 Ar-C), 130.44 (2 Ar-C), 132.85 (imidazole-C4), 133.67 (Ar-C), 142.50 (triazole-C4), 152.10 (imidazole-C2), 157.17 (imidazole-C5), 157.73 (pyridine-C6), 158.75 (pyridine-C2), 159.47 (Ar-C), 168.02 (pyridine-C4), 168.70 (C=O). MS for  $\text{C}_{28}\text{H}_{20}\text{N}_{10}\text{O}_5$  [ $\text{M}]^+$ :  $m/z = 576.1$  (24.38%). Calculated analysis for  $\text{C}_{28}\text{H}_{20}\text{N}_{10}\text{O}_5$  (576.16): C, 58.33; H, 3.50; N, 24.30%. Found: C, 58.15; H, 3.42; N, 24.43%.

#### 2.4.2. Imidazole-triazole-pyridine hybrid (7b)

Yield = 0.81 g (66.8%), m.p. = 269-270°C. IR ( $\nu/\text{cm}^{-1}$ ): 1646 (C=O), 1681 (C=O), 2214 (C=N), 3346, 3208 (-NH<sub>2</sub>). <sup>1</sup>H NMR ( $\delta/\text{ppm}$ ): 2.61 (s, 3H, imidazole-CH<sub>3</sub>), 3.77 (s, 3H, -OCH<sub>3</sub>), 4.96 (s, 2H, N-CH<sub>2</sub>-CO), 5.20 (s, 2H, O-CH<sub>2</sub>-), 7.06 (d,  $J = 9.0$  Hz, 2H), 7.15 (d,  $J = 8.5$  Hz, 2H), 7.51 (d,  $J = 9.0$  Hz, 2H), 7.58 (d,  $J = 8.5$  Hz, 2H), 7.87 (s, 2H, NH<sub>2</sub>), 8.10 (s, 1H, imidazole-H), 8.32 (s, 1H, triazole-H). <sup>13</sup>C NMR ( $\delta/\text{ppm}$ ): 13.01 (CH<sub>3</sub>), 52.30 (-CH<sub>2</sub>-CO-), 55.90 (-O-CH<sub>3</sub>), 61.25 (-O-CH<sub>2</sub>-), 75.21 (pyridine-C5), 111.35 (pyridine-C3), 114.54 (2 Ar-C), 114.86 (2 Ar-C), 115.78 (2 -C=N), 123.04 (triazole-C5), 125.83 (Ar-C), 126.51 (Ar-C), 128.97 (2 Ar-C), 130.38 (2 Ar-C), 132.81 (imidazole-C4), 142.43 (triazole-C4), 152.15 (imidazole-C2), 157.22 (imidazole-C5), 157.60 (pyridine-C6), 158.46 (pyridine-C2), 159.13 (Ar-C), 159.52 (Ar-C), 168.11 (pyridine-C4), 168.67 (C=O). MS for C<sub>29</sub>H<sub>22</sub>N<sub>10</sub>O<sub>6</sub> [M]<sup>+</sup>:  $m/z = 606.3$  (20.76%). Calculated analysis for C<sub>29</sub>H<sub>22</sub>N<sub>10</sub>O<sub>6</sub> (606.17): C, 57.43; H, 3.66; N, 23.09%. Found: C, 57.56; H, 3.60; N, 23.01%.

#### 2.4.3. Imidazole-triazole-pyridine hybrid (7c)

Yield = 0.88 g (70.8%), m.p. > 300°C. IR ( $\nu/\text{cm}^{-1}$ ): 1670 (C=O), 1688 (C=O), 2218 (C=N), 3362, 3215 (-NH<sub>2</sub>). <sup>1</sup>H NMR ( $\delta/\text{ppm}$ ): 2.63 (s, 3H, imidazole-CH<sub>3</sub>), 4.98 (s, 2H, N-CH<sub>2</sub>-CO), 5.21 (s, 2H, O-CH<sub>2</sub>-), 7.10 (d,  $J = 9.0$  Hz, 2H), 7.60 (d,  $J = 8.5$  Hz, 2H), 7.78 (s, 2H, NH<sub>2</sub>), 7.87 (d,  $J = 8.0$  Hz, 2H), 8.11 (s, 1H, imidazole-H), 8.32 (s, 1H, triazole-H), 8.43 (d,  $J = 8.5$  Hz, 2H). <sup>13</sup>C NMR ( $\delta/\text{ppm}$ ): 13.07 (CH<sub>3</sub>), 52.27 (-CH<sub>2</sub>-CO-), 61.33 (-O-CH<sub>2</sub>-), 75.38 (pyridine-C5), 111.64 (pyridine-C3), 114.55 (2 Ar-C), 115.87 (2 -C=N), 122.85 (triazole-C5), 124.58 (2 Ar-C), 126.60 (Ar-C), 129.11 (2 Ar-C), 130.52 (2 Ar-C), 132.90 (imidazole-C4), 140.78 (Ar-C), 142.46 (triazole-C4), 143.95 (Ar-C), 152.13 (imidazole-C2), 157.18 (imidazole-C5), 157.81 (pyridine-C6), 159.01 (pyridine-C2), 159.41 (Ar-C), 168.15 (pyridine-C4), 168.74 (C=O). MS for C<sub>28</sub>H<sub>19</sub>N<sub>11</sub>O<sub>7</sub> [M]<sup>+</sup>:  $m/z = 621.2$  (31.04%). Calculated analysis for C<sub>28</sub>H<sub>19</sub>N<sub>11</sub>O<sub>7</sub> (621.15): C, 54.11; H, 3.08; N, 24.79%. Found: C, 54.31; H, 3.16; N, 24.91%.

#### 2.4.4. Imidazole-triazole-pyridine hybrid (7d)

Yield = 0.78 g (63.9%), m.p. = 284-285°C. IR ( $\nu/\text{cm}^{-1}$ ): 1665 (C=O), 1687 (C=O), 2217 (C=N), 3355, 3204 (-NH<sub>2</sub>). <sup>1</sup>H NMR ( $\delta/\text{ppm}$ ): 2.62 (s, 3H, imidazole-CH<sub>3</sub>), 4.96 (s, 2H, N-CH<sub>2</sub>-CO), 5.20 (s, 2H, O-CH<sub>2</sub>-), 7.10 (d,  $J = 8.5$  Hz, 2H), 7.53 (d,  $J = 8.5$  Hz, 2H), 7.64 (d,  $J = 8.5$  Hz, 2H), 7.71 (d,  $J = 8.5$  Hz, 2H), 7.84 (s, 2H, NH<sub>2</sub>), 8.08 (s, 1H, imidazole-H), 8.31 (s, 1H, triazole-H). <sup>13</sup>C NMR ( $\delta/\text{ppm}$ ): 13.01 (CH<sub>3</sub>), 52.34 (-CH<sub>2</sub>-CO-), 61.21 (-O-CH<sub>2</sub>-), 75.41 (pyridine-C5), 111.53 (pyridine-C3), 114.68 (2 Ar-C), 115.83 (2 -C=N), 122.90 (triazole-C5), 126.55 (Ar-C), 129.14 (2 Ar-C), 130.28 (2 Ar-C), 130.74 (2 Ar-C), 132.06 (Ar-C), 132.81 (imidazole-C4), 133.79 (Ar-C), 142.57 (triazole-C4), 151.98 (imidazole-C2), 157.26 (imidazole-C5), 157.70 (pyridine-C6), 158.78 (pyridine-C2), 159.45 (Ar-C), 168.08 (pyridine-C4), 168.75 (C=O). MS for C<sub>28</sub>H<sub>19</sub>ClN<sub>10</sub>O<sub>5</sub> [M]<sup>+</sup>:  $m/z = 610.4$  (27.85%). Calculated analysis for C<sub>28</sub>H<sub>19</sub>ClN<sub>10</sub>O<sub>5</sub> (610.12): C, 55.04; H, 3.13; N, 22.93%. Found: C, 55.16; H, 3.08; N, 22.86%.

#### 2.5. Ethyl 2-cyano-3-(4-((1-(2-(2-methyl-5-nitro-1H-imidazol-1-yl)-2-oxoethyl)-1H-1,2,3-triazol-4-yl)methoxy)phenyl)acrylate (9)

A mixture of 1-(2-azidoacetyl)-2-methyl-5-nitro-1H-imidazole (3) (0.94 g, 4.5 mmol) and ethyl 2-cyano-3-((4-propargyloxy)phenyl)acrylate (8) [16] (1.02 g, 4 mmol) was dissolved in 30 mL DMF. To the obtained solution, sodium ascorbate (40 mol %) and copper sulphate pentahydrate (20 mol %) had been introduced in sequence. The mixture was stirred at 35-40°C for 12 h and then diluted with 100 mL ice-cold water. The precipitate that formed was collected and washed with 5 mL of ethyl acetate to furnish the precursor, ethyl 2-(4-(triazolyl-methoxy)phenyl)acrylate compound 9.

Yield = 1.54 g (82.8%), m.p. = 145-146°C. IR ( $\nu/\text{cm}^{-1}$ ): 1721 (C=O), 1690 (C=O), 2218 (C=N). <sup>1</sup>H NMR ( $\delta/\text{ppm}$ ): 1.27 (t, 3H, OCH<sub>2</sub>CH<sub>3</sub>), 2.58 (s, 3H, imidazole-CH<sub>3</sub>), 4.25 (t, 2H, OCH<sub>2</sub>CH<sub>3</sub>), 4.92 (s, 2H, N-CH<sub>2</sub>-CO), 5.18 (s, 2H, O-CH<sub>2</sub>-triazole), 6.94 (d,  $J = 8.5$  Hz, 2H), 7.78 (d,  $J = 8.5$  Hz, 2H), 7.96 (s, 1H, CH=C-CN), 8.10 (s, 1H, imidazole-H), 8.25 (s,

1H, triazole-H). Calculated analysis for C<sub>21</sub>H<sub>19</sub>N<sub>7</sub>O<sub>6</sub> (465.14): C, 54.19; H, 4.11; N, 21.07%. Found: C, 54.30; H, 4.16; N, 21.12%.

#### 2.6. 1-Aryl-3,5-dicyano-6-hydroxy-4-(4-((1-(2-(2-methyl-5-nitro-1H-imidazol-1-yl)-2-oxoethyl)-1H-1,2,3-triazol-4-yl)methoxy)phenyl)-2-oxo-1,2-dihydropyridine hybrids 10a-d

An RB-flask (100 mL) was charged with a solution of ethyl 2-(4-(triazolyl-methoxy)phenyl)acrylate compound 9 (0.93 g, 2 mmol) in 30 mL of ethanol and piperidine (0.1 mL). The corresponding N-aryl cyanoacetamide compound 6a, 6b, 6c, or 6d [15] (2 mmol) was added, and the mixture was refluxed for 2 h. The obtained solid was filtered and crystallized from an EtOH/DMF mixture (4:1) to afford the corresponding imidazole-triazole-pyridine hybrids 10a, 10b, 10c, and 10d, respectively.

##### 2.6.1. Imidazole-triazole-pyridine hybrid (10a)

Yield = 0.70 g (60.6%), m.p. = 277-278°C. IR ( $\nu/\text{cm}^{-1}$ ): 1658 (C=O), 1685 (C=O), 2220 (C=N), 3304 (O-H). <sup>1</sup>H NMR ( $\delta/\text{ppm}$ ): 2.58 (s, 3H, imidazole-CH<sub>3</sub>), 4.96 (s, 2H, N-CH<sub>2</sub>-CO), 5.21 (s, 2H, O-CH<sub>2</sub>-triazole), 7.12 (d,  $J = 8.5$  Hz, 2H), 7.34-7.40 (m, 5H), 7.58 (d,  $J = 8.5$  Hz, 2H), 8.06 (s, 1H, imidazole-H), 8.30 (s, 1H, triazole-H), 8.87 (s, 1H, O-H). <sup>13</sup>C NMR ( $\delta/\text{ppm}$ ): 13.14 (CH<sub>3</sub>), 52.43 (-CH<sub>2</sub>-CO-), 59.65 (pyridine-C5), 61.21 (-O-CH<sub>2</sub>-), 106.27 (pyridine-C3), 114.58 (2 Ar-C), 115.97 (2 -C=N), 122.80 (triazole-C5), 126.37 (Ar-C), 128.06 (Ar-C), 129.00 (2 Ar-C), 130.04 (2 Ar-C), 132.72 (2 Ar-C), 133.31 (imidazole-C4), 135.40 (Ar-C), 142.63 (triazole-C4), 152.17 (imidazole-C2), 157.08 (imidazole-C5), 158.76 (pyridine-C2), 159.93 (Ar-C), 165.71 (pyridine-C6), 167.10 (pyridine-C4), 168.55 (C=O). MS for C<sub>28</sub>H<sub>19</sub>N<sub>9</sub>O<sub>6</sub> [M]<sup>+</sup>:  $m/z = 577.3$  (36.08%). Calculated analysis for C<sub>28</sub>H<sub>19</sub>N<sub>9</sub>O<sub>6</sub> (577.15): C, 58.23; H, 3.32; N, 21.83%. Found: C, 58.06; H, 3.40; N, 21.73%.

##### 2.6.2. Imidazole-triazole-pyridine hybrid (10b)

Yield = 0.71 g (58.5%), m.p. = 291-292°C. IR ( $\nu/\text{cm}^{-1}$ ): 1656 (C=O), 1684 (C=O), 2215 (C=N), 3291 (O-H). <sup>1</sup>H NMR ( $\delta/\text{ppm}$ ): 2.61 (s, 3H, imidazole-CH<sub>3</sub>), 3.79 (s, 3H, -OCH<sub>3</sub>), 4.95 (s, 2H, N-CH<sub>2</sub>-CO), 5.21 (s, 2H, O-CH<sub>2</sub>-triazole), 7.06 (d,  $J = 9.0$  Hz, 2H), 7.18 (d,  $J = 8.5$  Hz, 2H), 7.52 (d,  $J = 8.5$  Hz, 2H), 7.60 (d,  $J = 8.5$  Hz, 2H), 8.08 (s, 1H, imidazole-H), 8.31 (s, 1H, triazole-H), 8.76 (s, 1H, O-H). <sup>13</sup>C NMR ( $\delta/\text{ppm}$ ): 13.21 (CH<sub>3</sub>), 52.37 (-CH<sub>2</sub>-CO-), 56.14 (-O-CH<sub>3</sub>), 59.73 (pyridine-C5), 61.30 (-O-CH<sub>2</sub>-), 106.18 (pyridine-C3), 114.64 (4 Ar-C), 115.84 (2 -C=N), 122.80 (triazole-C5), 126.45 (Ar-C), 129.38 (2 Ar-C), 129.96 (2 Ar-C), 131.02 (Ar-C), 133.34 (imidazole-C4), 142.55 (triazole-C4), 152.11 (imidazole-C2), 156.94 (imidazole-C5), 158.83 (pyridine-C2), 159.20 (Ar-C), 159.78 (Ar-C), 165.57 (pyridine-C6), 167.25 (pyridine-C4), 168.60 (C=O). MS for C<sub>29</sub>H<sub>21</sub>N<sub>9</sub>O<sub>7</sub> [M]<sup>+</sup>:  $m/z = 607.2$  (18.93%). Calculated analysis for C<sub>29</sub>H<sub>21</sub>N<sub>9</sub>O<sub>7</sub> (607.16): C, 57.33; H, 3.48; N, 20.75%. Found: C, 57.48; H, 3.54; N, 20.67%.

##### 2.6.3. Imidazole-triazole-pyridine hybrid (10c)

Yield = 0.93 (74.8%), m.p. > 300°C. IR ( $\nu/\text{cm}^{-1}$ ): 1664 (C=O), 1688 (C=O), 2214 (C=N), 3301 (O-H). <sup>1</sup>H NMR ( $\delta/\text{ppm}$ ): 2.63 (s, 3H, imidazole-CH<sub>3</sub>), 4.97 (s, 2H, N-CH<sub>2</sub>-CO), 5.22 (s, 2H, O-CH<sub>2</sub>-triazole), 7.11 (d,  $J = 8.5$  Hz, 2H), 7.58 (d,  $J = 8.5$  Hz, 2H), 7.85 (d,  $J = 8.5$  Hz, 2H), 8.11 (s, 1H, imidazole-H), 8.30 (s, 1H, triazole-H), 8.41 (d,  $J = 8.5$  Hz, 2H), 8.93 (s, 1H, O-H). MS for C<sub>28</sub>H<sub>18</sub>N<sub>10</sub>O<sub>8</sub> [M]<sup>+</sup>:  $m/z = 622.4$  (40.11%). Calculated analysis for C<sub>28</sub>H<sub>18</sub>N<sub>10</sub>O<sub>8</sub> (622.13): C, 54.02; H, 2.91; N, 22.50%. Found: C, 54.23; H, 3.00; N, 22.63%.

##### 2.6.4. Imidazole-triazole-pyridine hybrid (10d)

Yield = 0.86 g (70.3%), m.p. > 300°C. IR ( $\nu/\text{cm}^{-1}$ ): 1661 (C=O), 1685 (C=O), 2218 (C=N), 3287 (O-H). <sup>1</sup>H NMR ( $\delta/\text{ppm}$ ): 2.61 (s, 3H, imidazole-CH<sub>3</sub>), 4.95 (s, 2H, N-CH<sub>2</sub>-CO), 5.21 (s, 2H, O-CH<sub>2</sub>-triazole), 7.09 (d,  $J = 8.0$  Hz, 2H), 7.51 (d,  $J = 8.5$  Hz, 2H), 7.63 (d,  $J = 8.5$  Hz, 2H), 7.71 (d,  $J = 8.5$  Hz, 2H), 8.08 (s, 1H, imidazole-H), 8.30 (s, 1H, triazole-H), 8.81 (s, 1H, O-H). MS for C<sub>28</sub>H<sub>18</sub>ClN<sub>10</sub>O<sub>6</sub> [M]<sup>+</sup>:  $m/z = 611.3$  (33.26%). Calculated analysis for C<sub>28</sub>H<sub>18</sub>ClN<sub>10</sub>O<sub>6</sub> (611.11): C, 54.96; H, 2.96; N, 20.60%. Found: C, 54.80; H, 3.03; N, 20.51%.

## 2.7. DFT modeling

All density functional theory (DFT) calculations have been carried out using the Gaussian 09W software [17]. Geometrical optimization of isolated hybrids has been achieved at the B3LYP level of theory with the 6-311+G(d, p) basis set [18]. The optimized structures, frontier molecular orbitals (FMOs), and electronic parameters were resolved by GaussView [19].

## 2.8. Antimicrobial assay

The antimicrobial efficacy of the produced nitroimidazole derivatives was assessed by measuring both inhibition zones (IZ) and minimum inhibitory concentrations (MIC) against different pathogens. This encompassed Gram (+ve) bacteria, including *S. aureus* (ATCC 29213) and *B. subtilis* (ATCC 19659), Gram (-ve) bacteria like *S. typhimurium* (ATCC 13311) and *E. coli* (ATCC 25922), along with fungal strains such as *C. albicans* (ATCC 14053). The antibacterial agent was produced in a stock solution at a predetermined concentration. To establish a range of concentrations in the microtiter plate wells, the stock solution was serially diluted twice in the broth medium (Mueller-Hinton broth for bacteria and RPMI-1640 for fungi). The concentration range usually covers a number of orders of magnitude. A bacterial and fungal suspension's turbidity was adjusted to a certain McFarland standard in order to provide a standardized inoculum of the test microorganism. To ensure uniform dispersion, a set volume of the standardized inoculum was applied to each well of the microtiter plate. For eighteen to twenty-four hours, the microtiter 96-well plates were incubated at the proper temperature (30°C for fungus and 37°C for bacteria). Following incubation, the microtiter plate was examined to determine the MIC of the antimicrobial agent that prevents the bacteria from growing visibly. The reference drugs were selected based on their established clinical use and relevance to the test microbial strains. Chloramphenicol, a broad-spectrum antibiotic, and Cephalothin, a first-generation cephalosporin, were employed as standards for antibacterial assays to allow for comparison with general as well as resistant bacteria. The use of two classes of standards allows for a more relevant comparison of the potency of the synthesized hybrids. Cycloheximide, a potent inhibitor of eukaryotic protein synthesis, was used as the standard reference for antifungal assay against *C. albicans*. The results for the drug references Chloramphenicol, Cephalothin, and Cycloheximide, obtained under identical experimental conditions (see the supporting information file) [20]. All the antimicrobial assays were performed in triplicate to reduce opportunities for error and maximize reproducibility and reliability of data.

## 2.9. Molecular docking

Molecular docking experiments were performed to determine the binding of interactions, focusing on the binding affinities of the new nitroimidazole-hybrids towards PDB: 1BDD protein, utilizing M.O.E. 2019. The *E. coli* UDP-N-acetylenolpyruvoyl glucosamine reductase (MurB) enzyme (PDB: 1BDD) was selected as the molecular target for the docking experiments. MurB is a crucial enzyme in the cytoplasmic peptidoglycan biosynthetic pathway in bacteria, an activity that is not present in humans, and hence making it an interesting and validated target for novel antibacterial research [21]. The use of one, clearly defined bacterial target provides the opportunity for regular and comparative examination of the mode of binding of all the synthesized hybrids against a therapeutically useful protein. While the initial mechanism of native nitroimidazoles is bio-reduction, the hybrids here are novel chemical entities. Nitroimidazole unit in these compounds is a pharmacophore that modulates redox potential or adds new sites of interaction, but the primary postulated mechanism for the hybrid structure is inhibition of critical enzymes like MurB with assistance from triazole and pyridine units. Docking against MurB attempts to confirm this hypothesis. However, preparation of the protein included water and co-crystallized ligand removal, addition of hydrogen atoms, and the assignment of partial charges using the AMBER10: EHT force field. The geometries of the hybrids synthesized were energy-minimized using the MMFF94x force field. The binding site of the native ligand was utilized to define the docking site. Docking simulations were executed using the

Triangle Matcher placement method and London dG scoring function, followed by energy refinement using the Forcefield refinement method and GBVI/WSA dG scoring function. The conformations produced were compared based on binding affinity (S, kcal/mol) and interaction patterns with key amino acid residues.

## 3. Results and Discussion

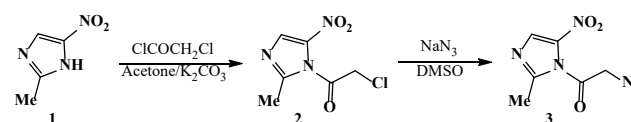
### 3.1. Preparation of imidazole-triazole-pyridine hybrids 7 and 10

The synthetic approach of our targeting imidazole-triazole-pyridine hybrids **7a-d** and **10a-d** is demonstrated in Schemes 1-3. This strategy is initiated by the preparation of the precursor, 1-(2-azidoacetyl)-2-methyl-5-nitro-1H-imidazole (**3**), by chloroacetylation of 2-methyl-5-nitro-1H-imidazole (**1**) upon treatment with chloroacetyl chloride in stirred acetone and potassium carbonate. The produced 1-(2-chloroacetyl)-2-methyl-5-nitro-1H-imidazole (**2**) was dissolved in dimethyl sulfoxide and stirred with sodium azide to furnish the corresponding 1-azidoacetyl-imidazole compound **3** (Scheme 1). The relatively low yield (54.6%) of compound **3** was accounted for by partial hydrolysis on aqueous workup. Different solvent systems and bases were tested; however, potassium carbonate and dry DMSO resulted in the maximum yield without decomposition.

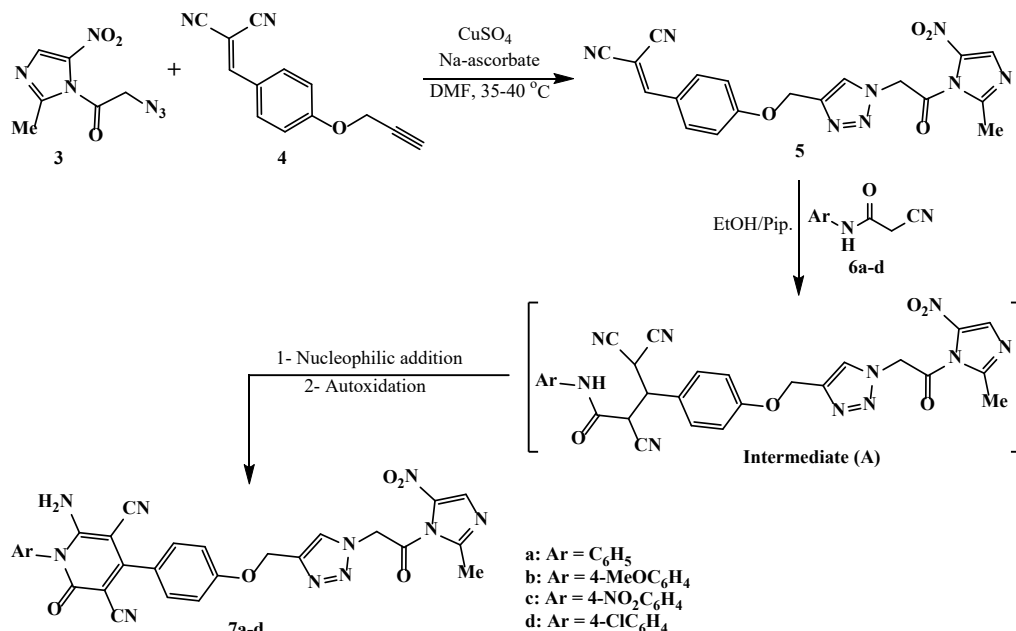
The azido-imidazole compound **3** has been employed as a precursor for the production of triazole ring system in the targeting 2-(4-(triazolyl-methoxy)benzylidene)-malononitrile compound **5** through its 1,3-dipolar cycloaddition reactions with the terminal alkyne, 2-((4-propargyloxy)benzylidene)malononitrile (**4**) °C in the presence of copper sulphate and sodium ascorbate in DMF as a solvent. The Huisgen cycloaddition reactions ran with pristine regioselectivity towards the 1,4-disubstituted triazole isomer, which was confirmed by the solo triazole proton resonance at  $\delta$  8.25-8.35 ppm and absence of any other triazole signals in the <sup>1</sup>H NMR spectra.

The 2-(4-(triazolyl-methoxy)benzylidene)-malononitrile compound **5** was refluxed with different *N*-aryl cyanoacetamide compounds **6a-d** [15] in ethanol and piperidine to produce the conforming imidazole-triazole-pyridine hybrids **7a-d** (Scheme 2). All the newly prepared hybrids **7a-d** were fully characterized using IR, <sup>1</sup>H NMR, <sup>13</sup>C NMR, and mass analyses. The mechanism was initiated by Michael in addition to the reaction of *N*-aryl cyanoacetamide compound **6** (donor) to unsaturated nitrile compound **5** (acceptor). The formed intermediate (**A**) underwent intramolecular addition of the N-H group of cyanacetamide part into the nitrile group and tautomerization, followed by air oxidation process to pick up the final targeted product, imidazole-triazole-pyridine hybrid **7**. The infrared spectrum of hybrid **7a** (as an example) revealed the characteristic absorption frequencies of carbonyl groups at 1651 and 1683 cm<sup>-1</sup>. The nitrile group (-C≡N) was detected at its expected frequency at 2211 cm<sup>-1</sup>. The absorptions of the amino function (-NH<sub>2</sub>) were observed at 3341 and 3213 cm<sup>-1</sup>. The <sup>1</sup>H NMR signals were detected as singlet signals at  $\delta$  2.61, 4.97, and 5.18 ppm for the protons of methyl (imidazole-CH<sub>3</sub>) and two methylene groups, respectively. The aromatic protons were identified by the doublet and multiplet signals at  $\delta$  7.10-7.56 ppm. The protons of the amino group were recorded by the singlet signal at  $\delta$  7.83 ppm. The detected singlet signals at  $\delta$  8.08 and 8.31 ppm were attributed to the protons of imidazole-C and triazole-C, respectively. The mass analysis displayed the molecular ion peak for the formula C<sub>28</sub>H<sub>20</sub>N<sub>10</sub>O<sub>5</sub> at *m/z* = 576.1 with a relative intensity of 24.38%.

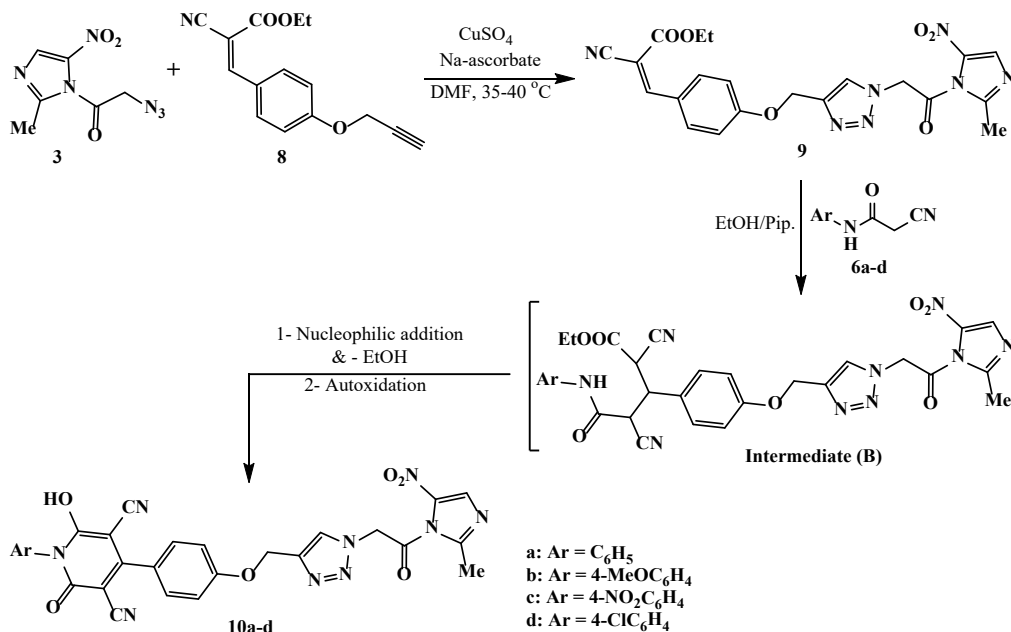
In Scheme 3, we aimed at replacing one of the nitrile functionalities in the first series with an ester group. Ethyl 2-(4-(triazolyl-methoxy)phenyl)acrylate compound **9** was synthesized in the same way that 2-(4-(triazolyl-methoxy)benzylidene)-malononitrile compound **5** was. Thereafter, the azido-imidazole compound **3** was further reacted with an ethyl 2-cyano-3-((4-propargyloxy)phenyl)acrylate (**8**) [16] through Azide-alkyne Huisgen cycloaddition to produce the target



Scheme 1. Synthesis of 1-(2-azidoacetyl)-2-methyl-5-nitro-1H-imidazole (**3**).



Scheme 2. Synthesis of imidazole-triazole-pyridine hybrids 7a-d.



Scheme 3. Synthesis of imidazole-triazole-pyridine hybrids 10a-d.

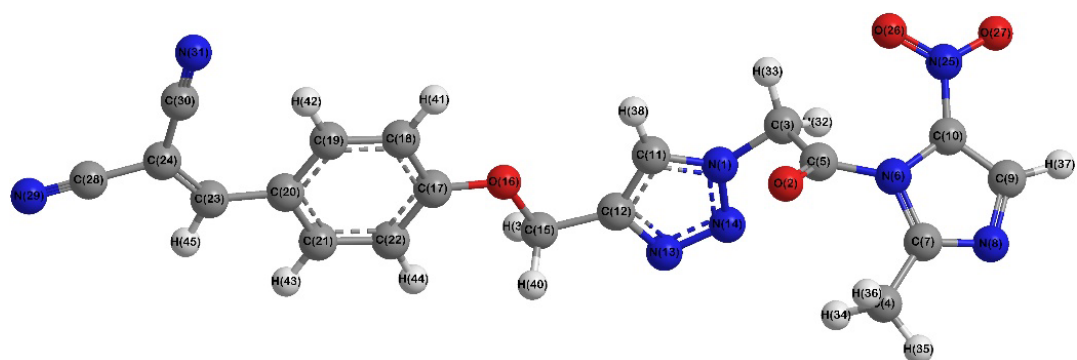
imidazole-triazole precursor **9**. Furthermore, the addition of *N*-aryl cyanoacetamide **6a-d** [15] to a refluxing solution of ethyl 2-(4-(triazolyl-methoxy)phenyl)acrylate compound **9** in ethanol and piperidine resulted in the formation of imidazole-triazole-pyridine hybrids of the type **10a-d**, in which the pyridine ring substituted with hydroxy group at position six (Scheme 3). The structure of the prepared hybrids of imidazole-triazole-pyridine **10a-d** was well characterized and confirmed through interpretation of the spectral analysis data. The IR spectrum of hybrid **10a** (as an example) exhibited absorption frequencies of carbonyl groups at 1658 and 1685 cm<sup>-1</sup>. The presence of nitrile and hydroxy groups was indicated by their expected frequencies at 2220 and 3304 cm<sup>-1</sup>, respectively. The <sup>1</sup>H NMR spectrum displayed the protons of protons of methyl (imidazole-CH<sub>3</sub>) and two methylene groups as singlet signals at δ 2.58, 4.96, and 5.21 ppm, respectively. The aromatic protons were identified by the doublet and multiplet signals at δ 7.12-7.58 ppm. The singlet signals at δ 8.06, 8.30, and 8.87

ppm were attributed to the protons of imidazole-C, triazole-C, and the hydroxy group, respectively.

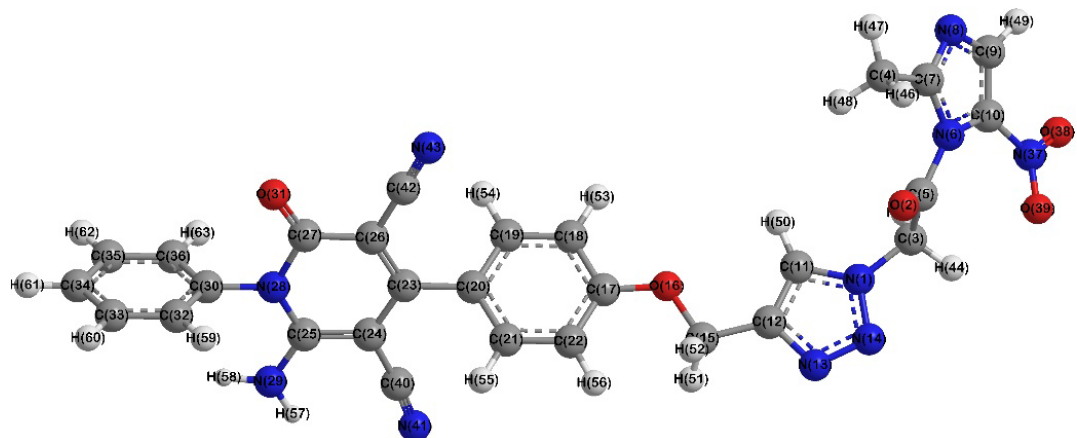
### 3.2. Molecular modeling

The nitroimidazole malononitrile **5** and acrylate **9**, along with their derivatives, amino-pyridyl **7a-d** and hydroxy-pyridyl **10a-d**, respectively, exhibited resemble non-planar structures (Figures 2-3). The dihedral angle data of these analogues revealed that:

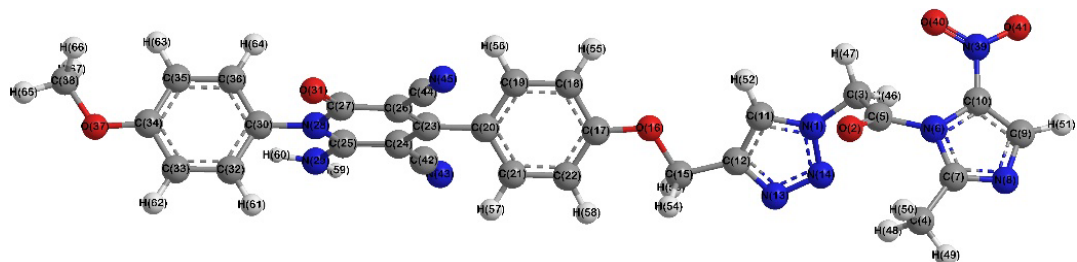
- The nitro-group atoms have been shifted away from the imidazole's plane, e.g., C<sup>2</sup><sub>(Imz)</sub>-N<sup>1</sup><sub>(Imz)</sub>-C<sup>5</sup><sub>(Imz)</sub>-NO<sub>2(Imz)</sub> ≈ -169.0°, whereas the methyl group displayed less shift (177.7°) (Table S1).
- Likewise, the oxoethyl atoms were dislocated from the imidazole and triazole planes, CO<sub>(OxEt)</sub>-N<sup>1</sup><sub>(Imz)</sub>-C<sup>2</sup><sub>(Imz)</sub>-N<sup>3</sup><sub>(Imz)</sub> ≈ 171.0°, CH<sub>2(OxEt)</sub>-CO<sub>(OxEt)</sub>-N<sup>1</sup><sub>(Imz)</sub>-C<sup>5</sup><sub>(Imz)</sub> ≈ 38.3°, C<sup>5</sup><sub>(Trz)</sub>-N<sup>1</sup><sub>(Trz)</sub>-CH<sub>2(OxEt)</sub>-CO<sub>(OxEt)</sub> ≈ 96.3° and CH<sub>2(OxEt)</sub>-N<sup>1</sup><sub>(Trz)</sub>-N<sup>2</sup><sub>(Trz)</sub>-N<sup>3</sup><sub>(Trz)</sub> ≈ 176.5°, respectively.



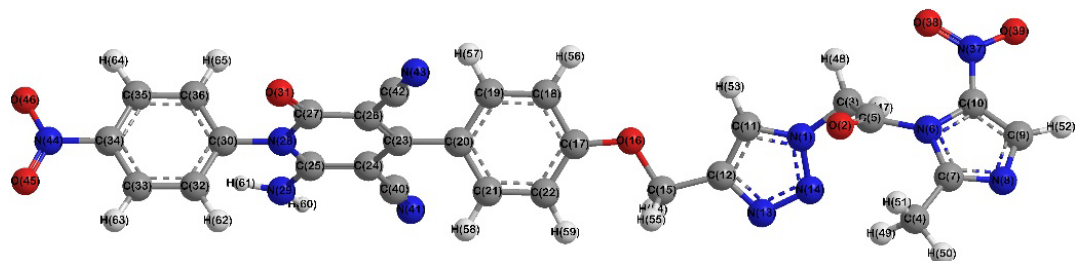
5



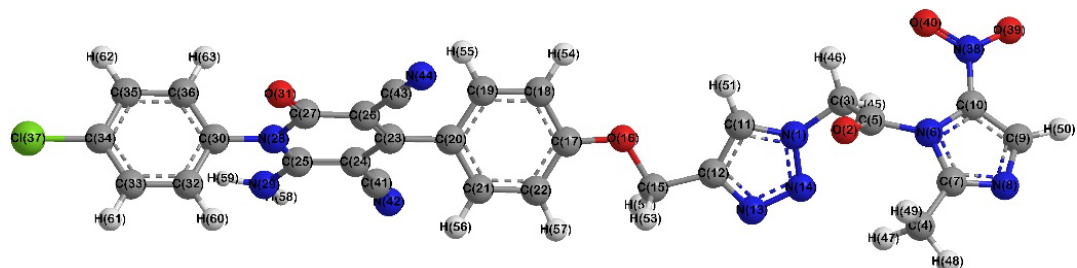
7a



7b



7c



7d

Figure 2. Compounds 5 and 7a-d optimized structures.

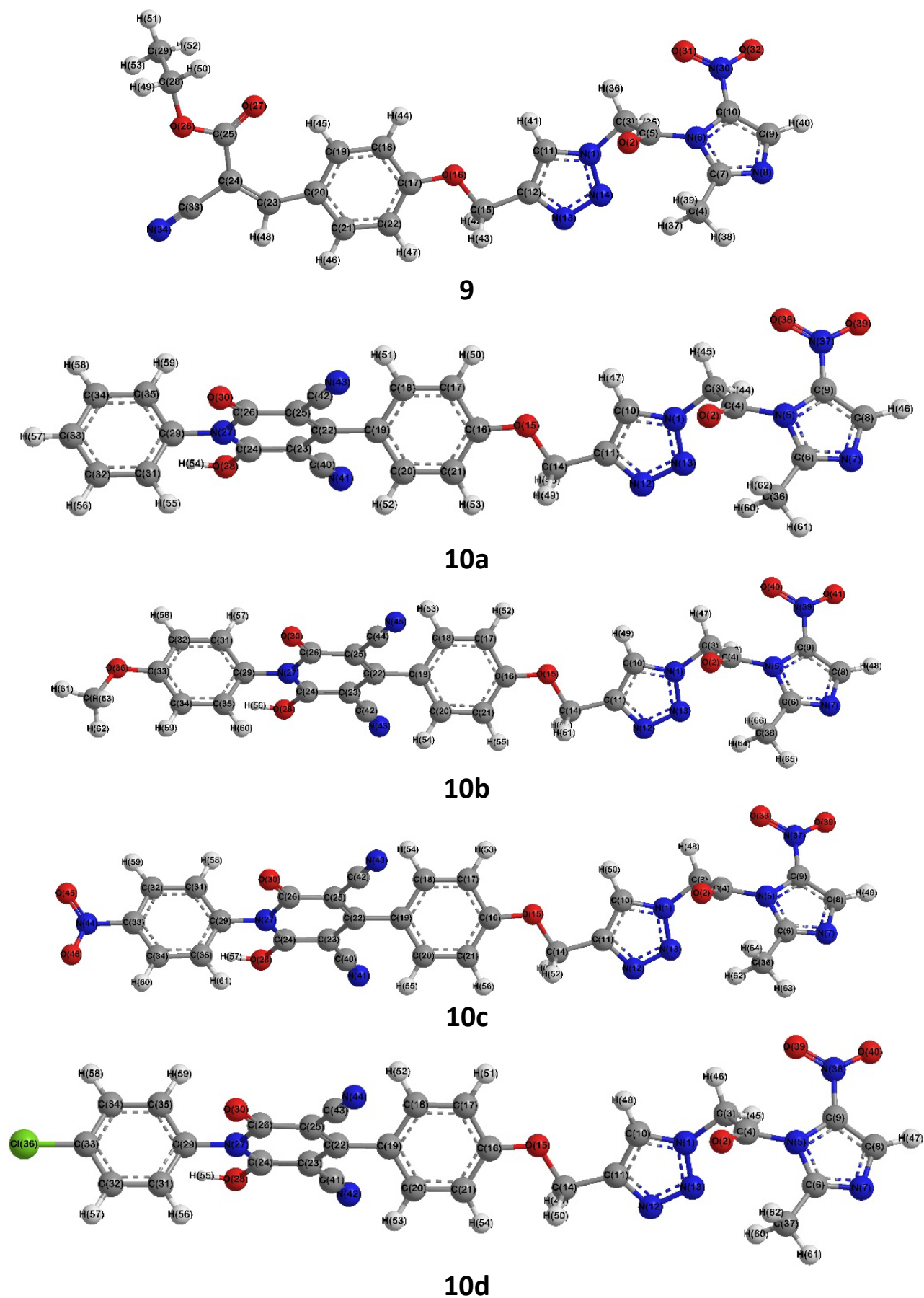


Figure 3. Compounds 9 and 10a-d optimized structures.

- iii) As well, the ether linkage has been positioned away the triazole's plane,  $N_{3(\text{Trz})}-C_{4(\text{Trz})}-CH_{2(\text{Ethr})}-O_{(\text{Ethr})} \approx -173.2^\circ$ , while it was coplanar with the phenyl ring, which was slanted on the pyridyl nucleus,  $C^2_{(\text{Ph})}-C^1_{(\text{Ph})}-C^4_{(\text{Py})}-C^3_{(\text{Py})} \approx -51.0^\circ$  (Table S1).
- iv) Otherwise, the two cyano- and oxo-substituents were slightly moved from the pyridyl's plane,  $C^5_{(\text{Py})}-C^4_{(\text{Py})}-CN^1_{(\text{Py})} \approx 176.9^\circ$  and  $C^3_{(\text{Py})}-C^4_{(\text{Py})}-CN^2_{(\text{Py})} \approx 176.2^\circ$ , while the oxo-, amino- and hydroxy groups were coplanar.
- v) Else, the phenyl substituent was practically perpendicular to the pyridyl ring,  $C^2_{(\text{Py})}-N^1_{(\text{Py})}-C^1_{(\text{PhPy})}-C^2_{(\text{PhPy})} \approx -91.8^\circ$ .

Moreover, the DFT estimated bond lengths and angles, in comparison to single crystal X-ray of comparable compounds [22], revealed a

valuable agreement as the discrepancies were  $<0.12 \text{ \AA}$  and  $<10.0^\circ$  (RMSD = 0.02-0.03 and 4.5-5.7), respectively. The disparity could be ascribed to that the DFT computations investigated a sole gaseous molecule where no columbic interactions (Tables S2-S3).

As they significantly manipulate the molecule's attitude to either afford or gain electrons [23], the HOMO-LUMO's energies, frontier molecular orbitals (FMOs), has gained noteworthy importance. The explored analogues displayed comparable configurations of their FMOs; for instance, the HOMO of nitroimidazole malononitrile 5 and acrylate 9 had been spanned on the phenyl malononitrile and acrylate, respectively, whereas their LUMO was confined on the oxoethyl nitroimidazole moiety (Figure 4 and S1). The corresponding amino-pyridyl 7a-d and hydroxy-pyridyl 10a-d displayed a coincided

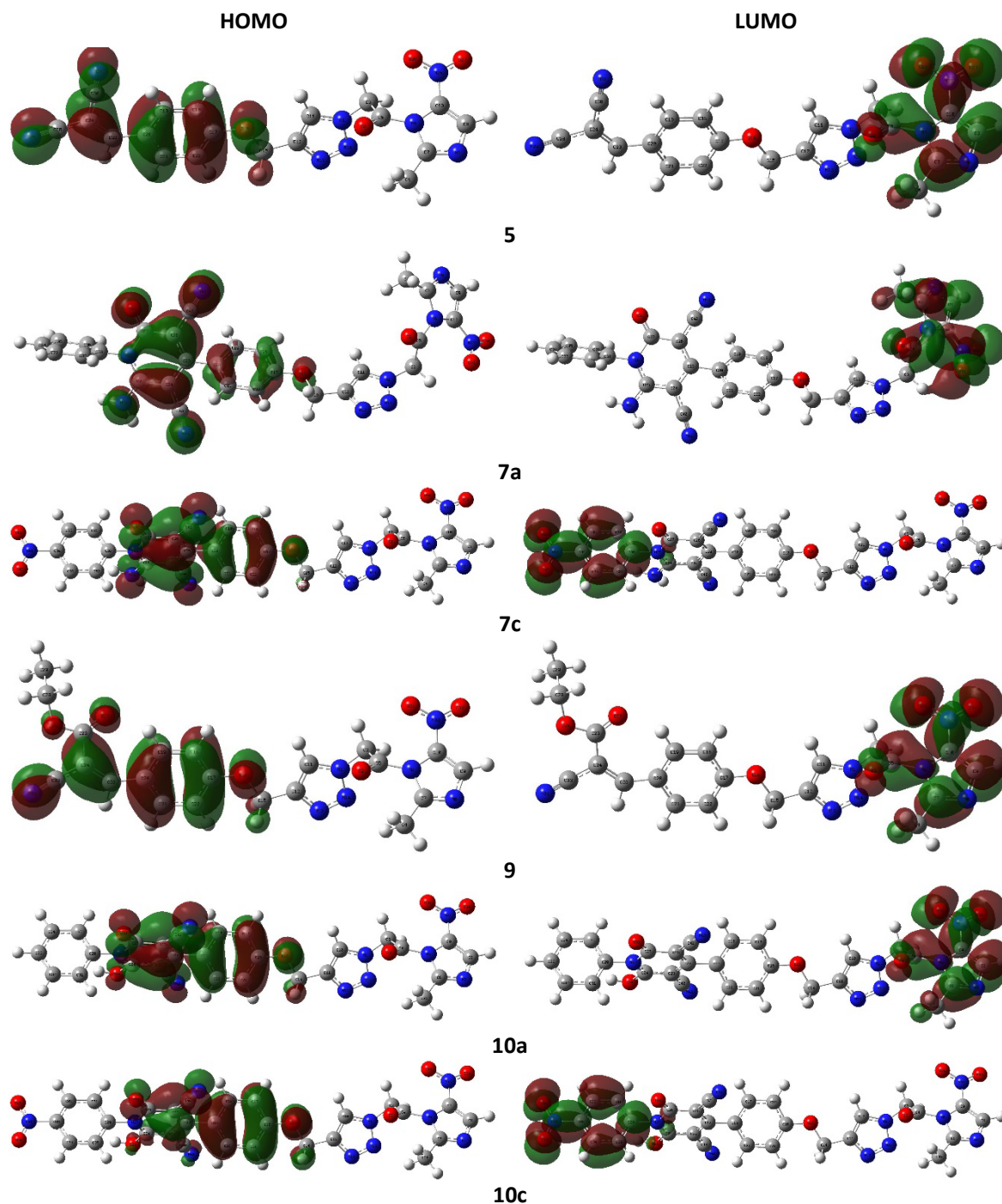


Figure 4. The 3D-plot of FMOs for compounds 5, 7a, 7c, 9, 10a, and 10c.

composition of the HOMO, which centered on the amino- and hydroxydicyanopyridyl methoxyphenyl fragment, and LUMO, which centered on the oxoethyl nitroimidazole moiety. The nitrophenyl derivatives **9c** and **10c** showed an alternative LUMO configuration, wherein centered on the nitrophenyl group (Figure 4 and S1).

Hence, the nitroimidazole analogues presented close values for the HOMO-LUMO energies,  $E_H = -6.96$  -  $-6.37$  and  $E_L = -3.75$  -  $-3.44$  eV, respectively. As a result, the observed energy gap ( $\Delta E_{H-L}$ ) was spanned from 2.93 to 3.33 eV, where the conjugates **7b** and **7a** had equal and the lowest value, while **5** exhibited the maximum, following the arrangement **7b** = **7a** < **7d** < **9** < **10c** < **10b** < **7c** < **10a** < **10d** < **5**. Accordingly, the data indicated that: i) the aminopyridyl hybrids **7** had lower energy gap than hydroxypyridyl's **10**; ii) In aminopyridyl series **7a-d**, the nitrophenyl (**7c**) exhibited the lowest energy gap, whereas the corresponding hydroxypyridyl (**10c**) had the maximum value; iii) In both cases, the following order was obeyed methoxyphenyl (b) < phenyl (a) < chlorophenyl (d) (Figure 5).

Moreover, the FMO's energy values have been exploited in the evaluation of particular chemical reactivity signifiers [24]. Such as, the electronegativity ( $\chi$ ) data divulged that conjugates **10c** and **7b** owned the highest and lowest standards (5.31 and 4.90 eV), respectively. Also, hybrid **5** unveiled the maximum hardness ( $\eta = 1.66$  eV) and minimum softness ( $\delta = 0.60$  eV). The electrophilicity index ( $\omega$ ), 8.01 (**10b**) - 9.07 (**10c**) eV, endorsed the satisfactory electrophilicity character of the hybrids,  $\omega > 1.5$  eV, with better tendency to deliver than receiving electrons, as they displayed lower electron donating ( $\omega^+$ ) than accepting ( $\omega^-$ ) power [25] (Table 1).

The molecule's charge-transfer and electronegativity may be comprehended more from studying the Mulliken's atomic charges [26]. The studied derivatives results unveiled that the imidazolyl nitrogen atoms  $N^1_{(Imz)}$  and  $N^3_{(Imz)}$  had alternative negative charges, -0.169 - -0.178 and -0.223 - -0.225, respectively. Likewise, the triazolyl nitrogen atoms  $N^2_{(Trz)}$  and  $N^3_{(Trz)}$  were negatively charged, while the

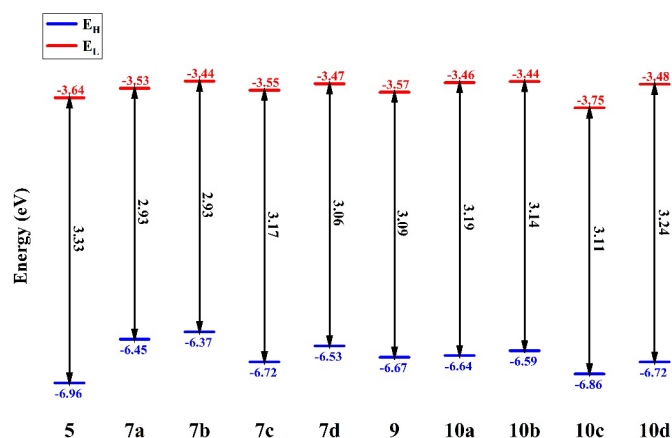


Figure 5. FMO's energy representation of explored hybrids.

Table 1. FMO's energies and reactivity descriptors (eV) of investigated compounds.

Compound	$E_H$	$E_L$	$\Delta E_{H-L}$	$\chi$	$\eta$	$\delta$	$\omega$	$\omega^+$	$\omega^-$
5	-6.96	-3.64	3.33	5.30	1.66	0.60	8.44	6.00	11.30
7a	-6.45	-3.53	2.93	4.99	1.46	0.68	8.50	6.19	11.18
7b	-6.37	-3.44	2.93	4.90	1.46	0.68	8.22	5.95	10.85
7c	-6.72	-3.55	3.17	5.13	1.59	0.63	8.31	5.94	11.07
7d	-6.53	-3.47	3.06	5.00	1.53	0.65	8.18	5.87	10.87
9	-6.67	-3.57	3.09	5.12	1.55	0.65	8.47	6.10	11.22
10a	-6.64	-3.46	3.19	5.05	1.59	0.63	8.01	5.68	10.73
10b	-6.59	-3.44	3.14	5.02	1.57	0.64	8.01	5.69	10.71
10c	-6.86	-3.75	3.11	5.31	1.55	0.64	9.07	6.61	11.91
10d	-6.72	-3.48	3.24	5.10	1.62	0.62	8.01	5.67	10.77

nitrogen  $N^1_{(Trz)}$  exhibited a small positive charge (0.014-0.016), which may be attributed to the electron-withdrawing influence of the bonded oxoethyl group ( $O_{(OxEt)} = -0.267$  -  $-0.271$ ) (Table S4). Moreover, the imidazolyl nitro-group acquired different charges, where the nitrogen  $NO_{2(Imz)}$  was positively charged (0.345), and the oxygen atoms had close negative charges ( $O^1_{(Imz)} = -0.362$  and  $O^2_{(Imz)} = -0.307$ ). Also, the ether oxygen  $O_{(Ethr)}$  gained a negative charge (-0.352), which is clearly higher than the corresponding oxoethyl atom. In compounds **5** and **9**, the cyano-groups nitrogen atoms have been negatively charged,  $NC^1_{(Min)} = -0.147$ ,  $NC^2_{(Min)} = -0.156$ , and  $NC_{(Acr)} = -0.172$ , respectively. Comparably, the cyano-groups nitrogen atoms in aminopyridyl conjugates **7a-d** exhibited higher charge than the corresponding in parent **5**,  $NC^1_{(Py)} = -0.173$  -  $-0.181$  and  $NC^2_{(Py)} = -0.185$  -  $-0.193$ , while those belonging to hydroxypyridyl's displayed lower values, -0.166 - -0.175. Further, the pyridyl ring substituents data revealed that the oxo-atom had the lower negative charge ( $O_{x(Py)} = -0.355$ ) than the hydroxy-oxygen and amino-nitrogen ( $OH_{(Py)} = -0.494$  and  $NH_{2(Py)} = -0.766$ ), respectively (Table S4).

Elsewhere, the hybrids' molecular polarizability ( $\alpha_{total}$ ), hyperpolarizabilities ( $\beta_{total}$ ), and dipole moment ( $\mu$ ) were appraised [27] to afford an illustration of the electronic density distribution (Eq. 1) and softness, which essentially influence the intermolecular interactions [28] (Eqs. 1 and 2).

$$\mu = (\mu_x^2 + \mu_y^2 + \mu_z^2) \quad \alpha_{total} = \frac{(\alpha_{xx} + \alpha_{yy} + \alpha_{zz})}{3} \quad (1)$$

$$\beta_{total} = \sqrt{(\beta_{xxx} + \beta_{yyy} + \beta_{zzz})^2 + (\beta_{yyy} + \beta_{zzz} + \beta_{xxx})^2 + (\beta_{zzz} + \beta_{xxx} + \beta_{yyy})^2} \quad (2)$$

The nitroimidazole derivatives unveiled widespread dipole moment ( $\mu$ ) oscillated from 2.70 D (**10c**) to 8.81 D (**7b**), which represented 1.97-6.42 times of urea, reference material (Table 2). Whilst, the analog **5** displayed the minimum polarizability value, but the conjugate **7c** possessed the utmost,  $\alpha_{total} = 3.23$  and  $4.26 \times 10^{-23}$  esu, respectively. On the contrary, the first-order hyperpolarizability suggested that compound **10c** has the minimum value ( $\beta_{total} = 4.50 \times 10^{-30}$  esu) and the analogue **10b** has the top ( $\beta_{total} = 15.72 \times 10^{-30}$  esu). In contrast to the urea's value (Ahmed et al., 2008), most of the considered conjugates presented larger hyperpolarizability, 12.02-41.93 times (Table 2).

### 3.3. Antimicrobial assay

The antimicrobial investigation for the nitroimidazole-hybrids was carried out and revealed significant variations in activity based on structural changes (Table 3). Meanwhile, nitroimidazole-hybrid **5** revealed proper antimicrobial effectiveness against *S. aureus*, *B. subtilis*, and *E. coli*, through an MIC = 12.5  $\mu\text{g.mL}^{-1}$  and IZ value = 39 mm, while showing lower effectiveness towards *S. typhimurium* (MIC = 50  $\mu\text{g.mL}^{-1}$ ) and *C. albicans* (MIC = 50  $\mu\text{g.mL}^{-1}$ ). This proposes moderate effectiveness, especially against Gram (+ve) bacteria. However, through the series **7a-d**, nitroimidazole-hybrid **7a** showed the strongest effectiveness among the examined hybrids, an MIC of 12.5  $\mu\text{g.mL}^{-1}$

Table 2. The dipole moment ( $\mu$ ), polarizability ( $\alpha_{total}$ ), polarizability anisotropy ( $\Delta\alpha$ ), and first-order hyperpolarizability ( $\beta_{total}$ ) of the explored hybrids.

Compound	M (Debye)	$\mu/\mu_{urea}$	$\alpha_{total}$ (esu $\times 10^{-23}$ )	$\Delta\alpha$ (esu $\times 10^{-23}$ )	$\beta_{total}$ (esu $\times 10^{-30}$ )	$\beta_{total}/\beta_{urea}$
5	6.87	5.00	3.23	1.18	11.43	30.58
7a	8.61	6.27	3.53	1.90	12.54	33.31
7b	8.81	6.42	3.54	1.93	13.91	37.23
7c	4.76	3.47	4.26	1.32	5.99	16.03
7d	6.45	4.70	3.83	1.48	5.55	14.86
9	3.68	2.68	3.25	1.09	4.83	12.92
10a	7.29	5.31	3.41	1.80	12.11	32.33
10b	8.69	6.33	3.51	1.89	15.72	41.93
10c	2.70	1.97	4.22	1.10	4.50	12.02
10d	5.50	4.00	3.80	1.45	6.63	17.72

**Table 3.** Inhibition zone (IZ; mm) and MIC ( $\mu\text{g}\cdot\text{mL}^{-1}$ ) results for the nitroimidazole-hybrids.

Hybrids	Gram +ve bacteria		Gram -ve bacteria		Fungi
	<i>S. aureus</i>	<i>B. subtilis</i>	<i>E. coli</i>	<i>S. typhimurium</i>	<i>C. albicans</i>
5	12.5±0.12 (39±0.53)	12.5±0.47 (39±0.39)	12.5±0.08 (34±1.01)	50±0.63 (47±1.21)	50±0.33 (39±1.25)
7a	6.25±0.06 (40±0.33)	6.25±0.19 (43±0.63)	12.5±0.43 (46±0.81)	25±0.33 (52±1.40)	100±0.58 (44±1.03)
7b	6.25±0.43 (37±0.52)	6.25±0.03 (33±0.29)	12.5±0.19 (39±0.42)	12.5±0.02 (43±0.36)	12.5±0.55 (40±1.62)
7c	50±0.29 (44±0.18)	12.5±0.18 (38±0.17)	50±0.63 (47±1.06)	100±0.64 (54±0.17)	100±0.82 (49±0.07)
7d	50±0.17 (36±0.47)	12.5±0.35 (44±0.53)	12.5±0.44 (40±1.28)	50±0.08 (43±1.09)	100±0.29 (39±0.63)
9	12.5±0.19 (33±0.05)	6.25±0.73 (28±1.02)	12.5±0.01 (35±1.33)	50±0.46 (39±0.33)	3.125±0.37 (41±1.33)
10a	12.5±0.03 (38±0.29)	12.5±0.11 (39±1.33)	25±0.96 (45±0.43)	50±0.32 (48±0.28)	100±0.46 (42±0.05)
10b	25±0.76 (36±0.30)	12.5±0.12 (37±1.08)	12.5±0.41 (42±1.06)	50±0.61 (46±1.02)	100±0.39 (31±0.53)
10c	50±0.91 (39±0.01)	6.25±0.49 (41±1.62)	6.25±0.35 (49±0.17)	6.25±0.06 (44±0.38)	50±0.07 (35±1.22)
10d	6.25±0.53 (33±0.44)	3.125±0.66 (30±1.23)	3.125±0.08 (42±1.09)	12.5±0.16 (46±0.01)	12.5±0.48 (33±0.03)
Chloramphenicol	6.25±0.11 (32±0.23)	6.25±0.05 (31±1.27)	3.125±0.80 (44±0.39)	6.25±0.21 (45±0.04)	–
Cephalothin	6.25±0.34 (34±0.12)	6.25±0.05 (34±1.17)	3.125±0.77 (41±1.02)	3.125±0.10 (43±0.02)	–
Cycloheximide	–	–	–	–	3.125±0.14 (39±0.31)

MIC and IZ values are presented as the mean  $\pm$  standard deviation (n = 3).

MIC and IZ values of 46–52 mm, indicating strong efficacy. However, through the series **7a-d**, nitroimidazole-hybrid **7a** showed the strongest effectiveness among the examined hybrids, with MIC = 6.25  $\mu\text{g}\cdot\text{mL}^{-1}$  versus *S. aureus* and *B. subtilis*, MIC = 12.5  $\mu\text{g}\cdot\text{mL}^{-1}$  towards *E. coli*, MIC = 25  $\mu\text{g}/\text{mL}$  versus *S. typhimurium*, and IZ values of 46–52 mm, suggesting enhanced potency due to structural modifications. Nitroimidazole-hybrid **7b** demonstrated similar antibacterial activity to nitroimidazole-hybrid **7a** (MIC = 6.25–12.5  $\mu\text{g}\cdot\text{mL}^{-1}$  and IZ = 33–43 mm), suggesting its potential as a versatile antimicrobial agent. Nitroimidazole-hybrid **7c**, despite showing high inhibition zones, exhibited weaker effectiveness overall, with MIC = 50  $\mu\text{g}\cdot\text{mL}^{-1}$  against *S. aureus* and *E. coli*, and MIC = 100  $\mu\text{g}\cdot\text{mL}^{-1}$  vs. *S. typhimurium* and *C. albicans*, proposing reduced in activity due to structural differences. Nitroimidazole-hybrid **7d** revealed a slight improvement in the activity compared to nitroimidazole-hybrid **7c**, with MIC values ranged from 12.5 to 50  $\mu\text{g}\cdot\text{mL}^{-1}$  against bacteria but was weak against *C. albicans* (MIC = 100  $\mu\text{g}\cdot\text{mL}^{-1}$ ). Nitroimidazole-hybrid **9** developed as the strongest antifungal agent, unveiling a forceful MIC = 3.125  $\mu\text{g}\cdot\text{mL}^{-1}$  against *C. albicans* comparable to the cycloheximide reference. Nitroimidazole-hybrid **9** also showed strong efficacy vs. *B. subtilis* (MIC = 6.25  $\mu\text{g}\cdot\text{mL}^{-1}$ ), with modest effects against other established bacteria. Among the series **10a-d**, nitroimidazole-hybrid **10a** showed a moderate antibacterial effectiveness, with MIC = 12.5  $\mu\text{g}\cdot\text{mL}^{-1}$  against Gram (+ve) bacteria and MIC values from 25 to 50  $\mu\text{g}\cdot\text{mL}^{-1}$  towards Gram (-ve) bacteria, even though disclosing weak antifungal effectiveness (MIC = 100  $\mu\text{g}\cdot\text{mL}^{-1}$ ). Nitroimidazole-hybrid **10b** exhibited slightly weaker antibacterial effectiveness, mainly against *S. aureus* (MIC = 25  $\mu\text{g}\cdot\text{mL}^{-1}$ ), while sustaining adequate Gram-negative bacterial inhibition. Nitroimidazole-hybrid **10c** displayed enhanced activity against *E. coli* (MIC = 6.25  $\mu\text{g}\cdot\text{mL}^{-1}$ ) and *S. typhimurium* (MIC = 6.25  $\mu\text{g}\cdot\text{mL}^{-1}$ ), making it one of the most effective Gram (-ve) bacterial inhibitors, however, its antifungal effectiveness stay put sensible (MIC = 50  $\mu\text{g}\cdot\text{mL}^{-1}$ ). Nitroimidazole-hybrid **10d** recorded the wide-spectrum agent, with MIC = 3.125  $\mu\text{g}/\text{mL}$  against *B. subtilis* and *E. coli*, MIC = 6.25  $\mu\text{g}\cdot\text{mL}^{-1}$  against *S. aureus*, and MIC = 12.5  $\mu\text{g}\cdot\text{mL}^{-1}$  against *S. typhimurium* and *C. albicans*. This recommended that nitroimidazole-hybrid **10d** is recognized as a promising for further progress as a broad-spectrum antimicrobial agent.

Finally, a general trend relating the MIC and IZ values existed, whereby compounds with lower MICs (and consequently greater potency) tended to exhibit larger inhibition zones. A few exceptions to this trend for individual compound-strain combinations can be accounted for by differences that exist between the two assays. Disk diffusion (IZ) test measures the percentage of inhibition of diffusion and overall growth in agar medium, while the broth microdilution (MIC) test determines the exact lowest concentration that inhibits growth in liquid medium. Solubility of the compound, rate of diffusion through the agar, and specific growth kinetics in different media can cause discrepancies between the two tests.

### 3.4. Structural activity relationship

The antimicrobial effectiveness of the synthesized nitroimidazole-hybrids was prejudiced according to their structural alterations, especially the presence of electron-donating or withdrawing groups, and the functionalization of the dihydropyridine scaffold. Nitroimidazole-hybrid **5**, with a malononitrile moiety, demonstrated moderate antibacterial effectiveness over (MIC = 12.5  $\mu\text{g}/\text{mL}$ ) against Gram (+ve) and Gram (-ve) bacterial strains but was less effective towards fungi (*C. albicans*, MIC = 50  $\mu\text{g}\cdot\text{mL}^{-1}$ ), representing limited fungal effectiveness. Meanwhile, nitroimidazole-hybrid **7a**, including a dihydropyridine-3,5-dicarbonitrile core, exhibited enhanced antibacterial effectiveness, mainly towards *S. aureus*, *B. subtilis*, and *S. typhimurium*, indicating that the electron-rich aminopyridine group shows a responsibility in the bacterial inhibition. However, nitroimidazole-hybrid **7b** has an additional methoxyphenyl branch, maintaining equivalent effectiveness towards Gram (+ve) bacteria while viewing an improvement on the antifungal effectiveness (*C. albicans*, MIC = 12.5  $\mu\text{g}\cdot\text{mL}^{-1}$ ), indicating that the methoxy branch enhanced their fungal inhibition. On the other hand, nitroimidazole-hybrid **7c**, joining to a nitrophenyl group, presented a significant reduction in the antibacterial inhibition against *S. aureus* and *E. coli*, probable due to steric hindrance affecting bacterial penetration, whereas its antifungal effect remained weak. Likewise, nitroimidazole-hybrid **7d**, including a chlorophenyl moiety, retained moderate antibacterial effectiveness but demonstrated weaker antifungal inhibitions (*C. albicans*, MIC = 100  $\mu\text{g}/\text{mL}$ ), indicating that the electron-withdrawing chloro-group might limit fungal binding interactions. Systematic SAR evaluation of the N-aryl substituents of hybrids **7a-d** and **10a-d** is presented in Table 4. Data indicate that EDGs

**Table 4.** Summary of SAR for N-aryl substituents on antimicrobial activity.

Hybrids	N-aryl substituent	Electronic effect	Key antimicrobial observations
7a	Phenyl	Neutral	Good broad-spectrum antibacterial activity.
7b	4-Methoxyphenyl	E.D.G	Maintained antibacterial activity; improved antifungal activity.
7c	4-Nitrophenyl	E.W.G	Reduced antibacterial activity; weak antifungal activity.
7d	4-Chlorophenyl	E.W.G	Moderate antibacterial activity; weak antifungal activity.
10a	Phenyl	Neutral	Moderate antibacterial activity.
10b	4-Methoxyphenyl	E.D.G	Moderate antibacterial activity.
10c	4-Nitrophenyl	E.W.G	Potent anti-Gram-negative activity.
10d	4-Chlorophenyl	E.W.G	Excellent broad-spectrum activity (most potent)

like methoxy in hybrids **7b** and **10b** tended to maintain or even increase broad-spectrum activity, while potent EWGs like nitro in hybrids **7c** and **10c** tended to reduce antibacterial activity perhaps through a shift in electronic properties affecting binding with targets or intracellular penetration. Notably, the most potent broad-spectrum agent was the *p*-chlorophenyl analogue **10d** with a moderately EWG, suggesting that there needs to be an optimum level of electronic and steric effects to achieve maximum activity.

A clear relationship was observed between the DFT calculated parameters of the synthesized conjugates and their antimicrobial effectiveness. Compounds with smaller HOMO-LUMO energy gap separations ( $\Delta E_{H-L}$ ) and greater electrophilicity ( $\omega$ ) generally exhibited stronger inhibition effects, indicating that efficient charge transfer enhanced the interaction between the hybrid and microbial targets. For instance, the derivatives **7c** ( $\Delta E_{H-L} = 3.17$  eV,  $\omega = 8.31$  eV) and **7a** ( $\Delta E_{H-L} = 2.93$  eV,  $\omega = 8.50$  eV) displayed the most pronounced activity (44-54 mm), which can be attributed to their higher molecular softness and improved electron delocalization. On the other hand, the analogues **9** and **10b**, characterized by slightly wider energy gaps and lower  $\omega$  values, were less active. These observations suggest that molecular flexibility and high electrophilic character play key roles

in improving antimicrobial efficiency. Therefore, fine-tuning the electronic distribution across the  $\pi$ -conjugated system represents an effective strategy for enhancing biological performance within this hybrids framework.

### 3.5. Molecular docking

However, the molecular docking results highlighted on the bindings affinities and the interactions of the produced nitroimidazole-hybrids with the target PDB: 1BDD protein (Table S5). For molecular docking validation, a reference drug Cephalosporin was employed. This reference possesses the central  $\beta$ -lactam structure common to Cephalothin and is a known antibiotic inhibitor of penicillin-binding proteins (PBPs). Although not the main target of cephalosporins, docking set a baseline binding property and pattern for a recognized antibiotic class within the same protein scaffold utilized by our hybrids to enable a relative assessment of docking scores. Though the key of interactions includes (H-acceptor, H-donor,  $\pi$ - $\pi$  stacking, and pi-H) bonds with definite amino acids such as Lys5, Lys8, Asn4, Asn24, Asn44, Pro39, and Ser40. Nitroimidazole-hybrid **5** also exhibited strong binding (-7.1215 kcal/mol), interacting with Asn24 via a hydrogen bond (3.21 Å) (Figure 6).

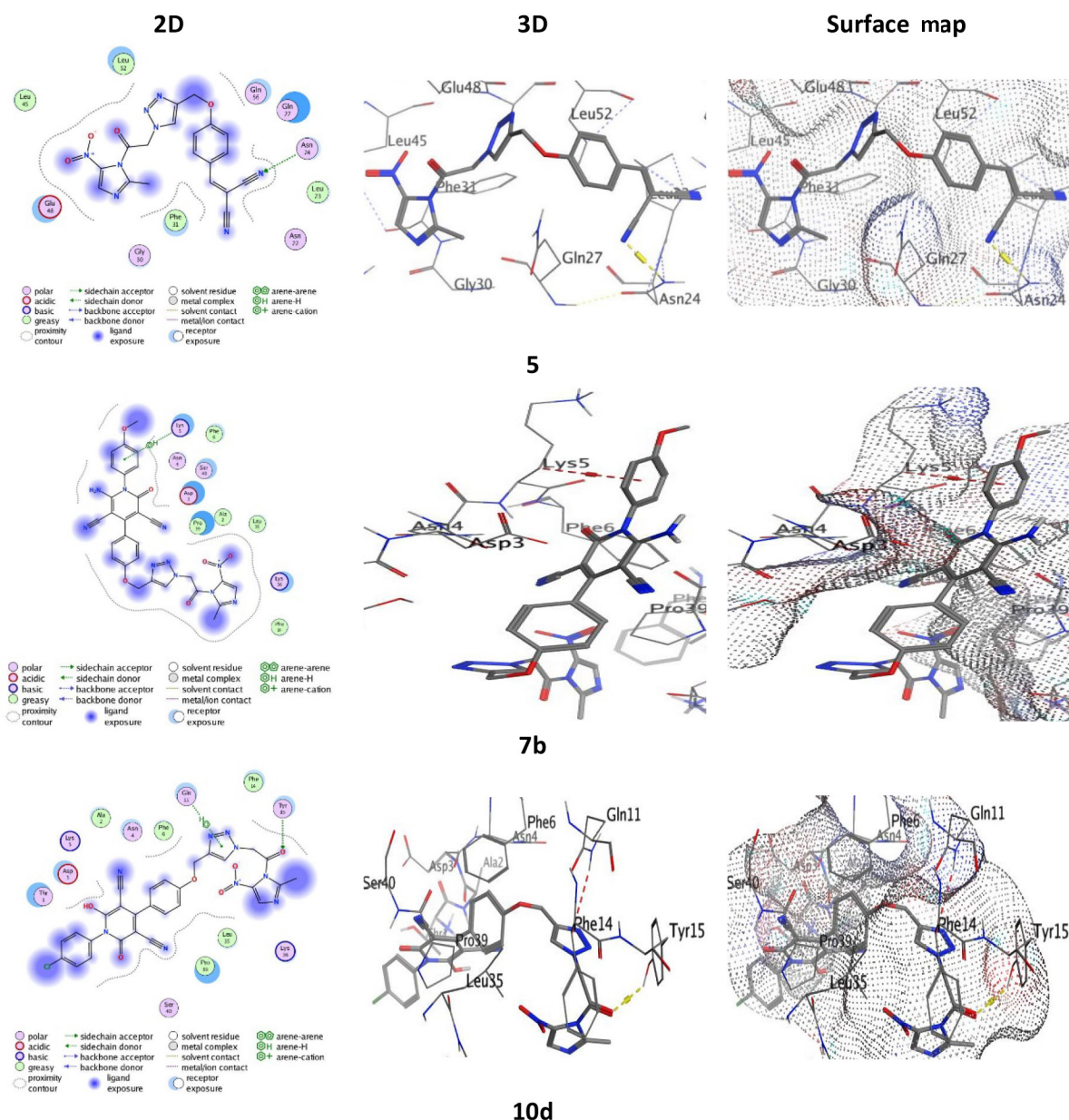


Figure 6. Binding images between nitroimidazole-hybrid **5**, **7b** and **10d** with PDB: 1BDD.

Nitroimidazole-hybrids **7a**, **7c**, and **7d** demonstrated multiple hydrogen bonds involving nitrile and triazole groups, with binding scores ( $S = -6.7898$ ,  $-6.9322$ , and  $-6.5246$  kcal/mol, respectively) (Figure S2). Meanwhile, the anisyl-ring in nitroimidazole-hybrid **7b** contributed to  $\pi$ -H interaction with Lys5, with a binding score ( $S = -7.0394$ ) (Figure 6).

Similarly, the imidazole-rings in nitroimidazole-hybrid **9** donated to  $\pi$ -H binding, over binding scores ( $S = -6.0546$  kcal.mol<sup>-1</sup>) with Leu52 (Figure S2). Moreover, nitroimidazole-hybrids **10a-c** showed moderate binding affinities ( $S = -6.5245$  to  $-6.3506$  kcal.mol<sup>-1</sup>), with interactions involving carbonyl and nitrile groups (Figure S2). However, nitroimidazole-hybrid **10d** developed as the most potent binder, with a strong docking score ( $S = -7.2123$  kcal.mol<sup>-1</sup>, forming a H-bond with Tyr15 (2.98 Å) and a  $\pi$ -H stacking with Gln11 (4.06 Å) (Figure 6). Furthermore, the reference drugs, Chloramphenicol and Cephalosporin, displayed lower binding affinities ( $S = -5.7485$  and  $-6.7186$  kcal.mol<sup>-1</sup>, respectively), primarily interacting with Ser40, Lys5, and Lys8 residues (Figure S2). These results suggest that the thiazolidinone-triazole hybrids, particularly those with nitrile and carbonyl groups, exhibit enhanced binding affinities and diverse interaction profiles compared to the reference compounds.

Finally, from the total SAR, docking data, and structural features, one can hypothesize an anticipated mechanism of action. The conserved nitroimidazole-triazole-oxoethyl chain appears to act as an anchor, potentially binding to the active site of the MurB enzyme, as predicted from docking. The dihydropyridine-N-aryl spacer domain variable is likely to control spectrum and potency; electron-donating systems, as in hybrid **7b** possibly prefer more extensive contacts, while specific EWGs (such as *p*-chloro moiety in hybrid **10d** can optimize fit as well as electronic complementarity in a sub-pocket to yield the resultant high potency. The imidazole nitro group, while not necessarily committed to its standard bio-reductive mechanism here, is participating in the electron affinity of the molecule and might be participating in significant hydrogen bonding or dipole interactions, as seen in the docking orientations with residues Asn24 and Tyr15.

### 3.6. Pharmacokinetic analysis

The SwissADME analysis of the novel nitroimidazole-hybrids revealed detailed pharmacokinetic properties, highlighting their potential as drug candidates (Table S6 and Figure S3). Nitroimidazole-hybrid **5** (M. Wt.: 418.37) exhibited high solubility, moderate lipophilicity (iLogP: 2.19), and a TPSA of 168.23 Å<sup>2</sup>, indicating good membrane permeability. With low GI absorption, no BBB permeability, and no Pgp substrate activity, it is suitable for peripheral targets, adhering to Lipinski's rule with one violation and achieving a bioavailability score of 0.55. Similarly, nitroimidazole-hybrid **9** (M. Wt.: 465.42) demonstrated high solubility, a favorable iLogP (2.5), and a TPSA of 170.74 Å<sup>2</sup>, with low GI absorption and no BBB permeability, making it a promising candidate for non-CNS applications. It also adhered to Lipinski's rule with one violation and scored 0.55 in bioavailability. In contrast, nitroimidazole-hybrids **7a-d** and **10a-d** displayed more complex profiles, with higher molecular weights (576.52–622.50), moderate solubility, and iLogP values ranging from 2.09 to 2.71. These compounds showed low GI absorption, no BBB permeability, and, except for nitroimidazole-hybrids **7b** and **10b**, were identified as Pgp substrates, which could limit their intracellular concentrations. Their TPSA values (210.46–262.07 Å<sup>2</sup>) and increased rotatable bonds (RT: 9–10) contributed to higher polarity and two Lipinski violations, resulting in uniformly low bioavailability scores (0.17). Among these hybrids, nitroimidazole-hybrid **7a** (M. Wt.: 576.52) and nitroimidazole-hybrid **10a** (M. Wt.: 577.51) revealed moderate-solubility and affirmative Pgp substrate, while nitroimidazole-hybrid **7b** (M. Wt.: 606.55) and hybrid **10b** (M. Wt.: 607.53) weren't Pgp substrates, hypothetically presenting recompenses for certain therapies. Nitroimidazole-hybrids **7c** (M. Wt.: 621.52) and **10c** (M. Wt.: 622.50) showed the highest molecular-weights and TPSA values, further dropping their bioavailability, however nitroimidazole-hybrids **7d** (M. Wt.: 610.97) and **10d** (M. Wt.: 611.95) reflected the profiles of nitroimidazole-hybrids **7a** and **10a**. While nitroimidazole-hybrids **5** and **9** stand displayed the most drug-like candidates, the nitroimidazole-hybrids **7a-d** and **10a-d** current chances for structural variation to improve their pharmacokinetic possessions, predominantly

for targeted therapies where Pgp effluence may be alleviated. This comprehensive analysis provides a foundation for further development of these hybrids as potential therapeutic agents.

## 4. Conclusions

The synthetic methodology for nitroimidazole-triazole-pyridine hybrids **7a-d** (substituted with an amino group at position-6 of pyridine) involves application of Huisgen cycloaddition reaction between 1-(2-azidoacetyl)-2-methyl-5-nitro-1*H*-imidazole (**3**) and the terminal alkyne, 2-((4-propargyloxy)benzylidene)malononitrile (**4**), followed by cyclization of the produced imidazole-triazole compound **5** with *N*-aryl cyanoacetamides **6a-d**. The second series **10a-d** (substituted with a hydroxy group at position-6 of pyridine) was successfully obtained from the reaction of azidoacetyl-imidazole compound **3** with ethyl 2-cyano-3-((4-propargyloxy)phenyl) acrylate (**8**), followed by cyclization of the produced imidazole-triazole compound **9** with *N*-aryl cyanoacetamides **6a-d**. The explored analogues displayed comparable configurations of their HOMO, spanned on the amino- or hydroxy-dicyanopyridyl methoxyphenyl fragment, and LUMO, confined on the oxoethyl nitroimidazole moiety, except for the nitrophenyl's **9c** and **10c**, wherein LUMO centered on the nitrophenyl group. However, the antimicrobial evaluation of the prepared nitroimidazole-hybrids **7a**, **7b**, and **10d** exhibited robust antibacterial effectiveness, predominantly towards Gram (+ve) bacteria, with MIC values as low as 3.125 to 6.25  $\mu\text{g.mL}^{-1}$ , making them equivalent to standard references. Meanwhile, nitroimidazole-hybrid **9** showed the highest antifungal effectiveness (MIC = 3.125  $\mu\text{g.mL}^{-1}$ ), like cycloheximide. Nitroimidazole-hybrid **10d** arisen as a wide-spectrum antimicrobial agent, revealing low MIC values against both Gram (+ve) and Gram (-ve) bacterial strains, as well as *C. albicans*. These antimicrobial results suggest that nitroimidazole-hybrids **7a**, **7b**, and **10d** are auspicious candidates, warranting further optimization and in vivo evaluation. In addition, the molecular docking study of thiazolidinone-triazole hybrids revealed significant binding affinities and diverse interaction mechanisms with the target protein. Nitroimidazole-hybrid **10d** exhibited the highest binding affinity ( $S = -7.2123$  kcal.mol<sup>-1</sup>), forming strong hydrogen bonds and  $\pi$ -H interactions. Nitroimidazole-hybrid **5** also demonstrated strong binding ( $S = -7.1215$  kcal/mol) through hydrogen bonding with Asn24. The nitrile and carbonyl groups in nitroimidazole-hybrids **7a**, **7c**, and **10b** facilitated multiple hydrogen bonds, while aromatic rings in nitroimidazole-hybrids **7b** and **9** contributed to  $\pi$ -H interactions. These findings highlight the potential of nitroimidazole-hybrids, particularly **10d** and **5**, as promising candidates for further development due to their superior binding affinities and interaction profiles compared to the reference compounds. The SwissADME prediction and biological profiling offer an orthogonal set of circumstances for lead selection. The nitroimidazole-hybrids **5** and **9** are reported to have excellent predicted drug-likeness and pharmacokinetic features and thus a very high chance of *in vivo* efficacy. As a contrast, nitroimidazole-hybrid **10d**, having a less desirable ADME profile (higher molecular weight, more Lipinski rule breaches), possesses greater and broad-spectrum antimicrobial activity. This illustrates one typical trade-off in drug discovery between pharmacokinetics and efficacy. Nitroimidazole-hybrid **10d** is a very promising lead compound whose very potent activity may justify medicinal chemistry optimization, such as prodrug strategies or structural simplification, to improve its pharmacokinetic profile without compromising its excellent efficacy. Overall, this study underscores the potential of imidazole-triazole-pyridine hybrids as therapeutic agents, with nitroimidazole-hybrids **5** and **9** standing out as particularly viable candidates for future investigation.

## CRedit authorship contribution statement

**Maha Ali Aljowni, Hind A. Siddiq:** Data curation, formal analysis, methodology, and software; **Rabah N Alsulami, Gadeer R. S. Ashour:** Investigation and writing – review & editing; **Nawaa Ali H. Alshammari, Adel I. Alalawy:** Formal analysis, investigation, writing-original draft; **Wael M. Alamoudi, Hana M. Abumelha:** Supervision and administration of research group.

## Declaration of competing interest

There are no conflicts of interest.

## Data availability

The data that support the findings of this study are available on request from the corresponding author.

## Declaration of generative AI and AI-assisted technologies in the writing process

The authors confirm that there was no use of artificial intelligence (AI)-assisted technology for assisting in the writing or editing of the manuscript and no images were manipulated using AI.

## Acknowledgment

Princess Nourah bint Abdulrahman University Researchers Supporting Project number (PNURSP2025R22), Princess Nourah bint Abdulrahman University, Riyadh, Saudi Arabia.

## Supplementary data

Supplementary material to this article can be found online at [https://dx.doi.org/10.25259/AJC\\_179\\_2025](https://dx.doi.org/10.25259/AJC_179_2025).

## References

- Muteeb, G., Rehman, M.T., Shahwan, M., Aatif, M., 2023. Origin of antibiotics and antibiotic resistance, and their impacts on drug development: A narrative review. *Pharmaceuticals (Basel, Switzerland)*, **16**, 1615. <https://doi.org/10.3390/ph16111615>
- De, S.S., Gupta, S.D., Degani, M.S. Nitroheterocyclics as anti-tuberculosis agents: An overview. In: *Frontiers in drug design and discovery, Frontiers in drug design and discovery: Volume 12*: Bentham Science Publishers), 96-174. <https://doi.org/10.2174/9789815165258123120005>
- Nepali, K., Lee, H.Y., Liou, J.P., 2019. Nitro-group-containing drugs. *Journal of Medicinal Chemistry*, **62**, 2851-2893. <https://doi.org/10.1021/acs.jmedchem.8b00147>
- Vichi-Ramirez, M.M., López-López, E., Soriano-Correa, C., Barrientos-Salcedo, C., 2024. Using 5-nitroimidazole derivatives against neglected tropical protozoan diseases: Systematic review. *Future Pharmacology*, **4**, 222-255. <https://doi.org/10.3390/futurepharmacol4010015>
- Kannigadu, C., N'Da, D.D., 2020. Recent advances in the synthesis and development of nitroaromatics as anti-infective drugs. *Current Pharmaceutical Design*, **26**, 4658-4674. <https://doi.org/10.2174/1381612826666200331091853>
- Gupta, R., Sharma, S., Singh, R., Vishwakarma, R.A., Mignani, S., Singh, P.P., 2022. Functionalized nitroimidazole scaffold construction and their pharmaceutical applications: A 1950–2021 comprehensive overview. *Pharmaceuticals*, **15**, 561. <https://doi.org/10.3390/ph15050561>
- Kumar, R.N., Mallareddy, G., Nagender, P., Rao, P.S., Poornachandra, Y., Ranjithreddy, P., Kumar, C.G., Narsaiah, B., 2016. Synthesis of novel triazole functionalized pyridine derivatives as potential antimicrobial and anti-biofilm agents. *Indian Journal of Chemistry*, **55B**, 1361-1375. <https://doi.org/10.1134/S107036321706024X>
- Sumrra, S.H., Suleman, A., Chohan, Z.H., Zafar, M.N., Raza, M.A., Iqbal, T., 2017. Triazole metal based complexes as antibacterial/antifungal agents. *Russian Journal of General Chemistry*, **87**, 1281-1287. <https://doi.org/10.1134/s107036321706024x>
- Tu, J., Sheng, C. Triazole antifungal drug—fluconazole. In: *Medicinal Chemistry and Drug Development*: Elsevier), 449-464. <https://doi.org/10.1016/B978-0-443-27402-2.00017-6>.
- Poyraz, S., Yıldırım, M., Ersatir, M., 2024. Recent pharmacological insights about imidazole hybrids: A comprehensive review. *Medicinal Chemistry Research*, **33**, 839-868. <https://doi.org/10.1007/s00044-024-03230-2>
- De, S., Kumar S K, A., Shah, S.K., Kazi, S., Sarkar, N., Banerjee, S., Dey, S., 2022. Pyridine: The scaffolds with significant clinical diversity. *RSC Advances*, **12**, 15385-15406. <https://doi.org/10.1039/d2ra01571d>
- Veselov, M.S., Ivanenkov, Y.A., Yamidanov, R.S., Osterman, I.A., Sergiev, P.V., Aladinskiy, V.A., Aladinskaya, A.V., Terentiev, V.A., Ayginin, A.A., Skvortsov, D.A., Komarova, K.S., Chemeris, A.V., Baimiev, A.K., Sofronova, A.A., Machulkin, A.E., Petrov, R.A., Maklakova, S.Y., Bezrukov, D.S., Filkov, G.I., Zainullina, L.F., Maximova, M.A., Zileeva, Z.R., Kartsev, V.G., Vakhitova, Y.V., Dontsova, O.A., 2020. Identification of pyrrolo-pyridine derivatives as novel class of antibacterials. *Molecular Diversity*, **24**, 233-239. <https://doi.org/10.1007/s11030-019-09946-3>
- Bhakta, A., Mukhtar, S., Anwar, S., Haider, S., Alahmdi, M.I., Parveen, H., Alsharif, M.A., Wani, M.Y., Chakrabarty, A., Hassan, M.I., 2024. Design, synthesis, molecular docking and anti-proliferative activity of novel phenothiazine containing imidazo [1, 2-a] pyridine derivatives against MARK4 protein. *RSC Medicinal Chemistry*, **15**, 1942-1958. <https://doi.org/10.1039/D4MD00059E>
- Lermontova, S.A., Lyubova, T.S., Grigoryev, I.S., Ilichev, V.A., Plekhanov, V.I., Shilyagina, N.Y., Balalaeva, I.V., Boyarskiy, V.P., Klapshina, L.G., 2023. Multifunctional photosensitizers for PDT and unique fluorescent sensors based on the new series of cyanoaryl porphyrazines with 4-(2-Propinyloxy)phenyl and 4-Benzyloxyphenyl fragments in a macrocycle framing. *Russian Journal of General Chemistry*, **93**, S672-S687. <https://doi.org/10.1134/s1070363223160053>
- Laliberté, R., Médawar, G., 1970.  $\beta$ -Ketoalkylthioacrylic acid derivatives as precursors of thiophenes, thiazolines, and thienopyrimidines. *Canadian Journal of Chemistry*, **48**, 2709-2717. <https://doi.org/10.1139/v70-457>
- Ramachary, D.B., Reddy, G.B., 2006. Towards organo-click reactions: Development of pharmaceutical ingredients by using direct organocatalytic bio-mimetic reductions. *Organic & Biomolecular Chemistry*, **4**, 4463-4468. <https://doi.org/10.1039/b612611a>
- Frisch, M., Trucks, G., Schlegel, H., Scuseria, G., Robb, M., Cheeseman, J., Scalmani, G., Barone, V., Mennucci, B., Petersson, G., 2009. Gaussian 09W, Gaussian, Inc., Wallingford, CT, USA.
- Becke, A.D., 1993. Density-functional thermochemistry. III. The role of exact exchange, *Journal of Chemical Physics*, **98**, 5648-5652. <https://doi.org/10.1063/1.464913>
- Dennington, R., Keith, T., Millam, J., 2009. GaussView, version 5, Semichem Inc., Shawnee Mission, KS.
- El-Gohary, N.S., Shaaban, M.I., 2017. Synthesis and biological evaluation of a new series of benzimidazole derivatives as antimicrobial, anti-quorum-sensing and antitumor agents. *European Journal of Medicinal Chemistry*, **131**, 255-262. <https://doi.org/10.1016/j.ejmech.2017.03.018>
- Mullaivendhan, J., Akbar, I., Gatasheh, M.K., Hatamleh, A.A., Ahamed, A., Abuthakir, M.H.S., Gurusamy, R., 2023. Cu (II)-catalyzed: Synthesis of imidazole derivatives and evaluating their larvicidal, antimicrobial activities with DFT and molecular docking studies. *BMC Chemistry*, **17**, 155. <https://doi.org/10.1186/s13065-023-01067-1>
- Zhang, L.Y., Tian, L.J., Zhang, C.F., 2007. 2-Phenyl-2H-1, 2, 3-triazole-4-carboxylic acid. *Acta Crystallographica Section E: Structure Reports Online*, **63**, o4415-o4415. <https://doi.org/10.1107/S1600536807051823>
- Bulat, F.A., Chamorro, E., Fuentealba, P., Toro-Labbé, A., 2004. Condensation of frontier molecular orbital fukui functions. *The Journal of Physical Chemistry A*, **108**, 342-349. <https://doi.org/10.1021/jp036416r>
- Xavier, S., Periandy, S., Ramalingam, S., 2015. NBO, conformational, NLO, HOMO-LUMO, NMR and electronic spectral study on 1-phenyl-1-propanol by quantum computational methods. *Spectrochimica Acta Part A: Molecular and Biomolecular Spectroscopy*, **137**, 306-320. <https://doi.org/10.1016/j.saa.2014.08.039>
- Afolabi, S.O., Semire, B., Akiode, O.K., Idowu, M.A., 2022. Quantum study on the optoelectronic properties and chemical reactivity of phenoxazine-based organic photosensitizer for solar cell purposes. *Theoretical Chemistry Accounts*, **141**. <https://doi.org/10.1007/s00214-022-02882-w>
- Bhagyasree, J.B., Varghese, H.T., Panicker, C.Y., Samuel, J., Van Alsenoy, C., Bolelli, K., Yildiz, I., Aki, E., 2013. Vibrational spectroscopic (FT-IR, FT-Raman, (1) H NMR and UV) investigations and computational study of 5-nitro-2-(4-nitrobenzyl) benzoxazole. *Spectrochimica acta. Part A, Molecular and Biomolecular Spectroscopy*, **102**, 99-113. <http://dx.doi.org/10.1016/j.saa.2012.09.032>
- Sun, Y., Chen, X., Sun, L., Guo, X., Lu, W., 2003. Nanoring structure and optical properties of GaAs8. *Chemical Physics Letters*, **381**, 397-403. <https://doi.org/10.1016/j.cplett.2003.09.115>
- Aziz, M., Ejaz, S.A., Tamam, N., Siddique, F., Riaz, N., Qais, F.A., Chtita, S., Iqbal, J., 2022. Identification of potent inhibitors of NEK7 protein using a comprehensive computational approach. *Scientific Reports*, **12**, 6404. <https://doi.org/10.1038/s41598-022-10253-5>